Acta Geologica Sinica (English Edition), 2019, 93(5): 1281–1299

Permian Tectonic Evolution in the Middle Part of Central Asian Orogenic Belt: Evidence from Newly Identified Volcanic Rocks in the Bilutu Area, Inner Mongolia

WANG Shijie[1], LIU Yang[2], DONG Xiaojie[1, *], XU Zhongyuan[1], WANG Wenlong[2], LI Shichao[1], SHI Qiang[1] and CUI Weilong[3]

[1] *College of Earth Science, Jilin University, Changchun 130061, China*
[2] *Tianjin Center of Geological Survey, China Geological Survey, Tianjin 300170, China*
[3] *State Key Laboratory of Lithospheric Evolution, Institute of Geology and Geophysics, Chinese Academy of Sciences, Beijing 100029, China*

Abstract: In this study, zircon U-Pb ages, geochemical and Lu-Hf isotopic data are presented for the newly identified volcanic rocks which were considered as Bainaimiao group in Bainaimiao Arc Belt (BAB), Inner Mongolia, which could provide important constraints on the evolution of the northern part of North China Block (NCB) and BAB. Basalt to basaltic andesite and andesite to dacite were collected from two sections, which showed eruption ages of 278.2±4.1 Ma and 258.3±3.0 Ma respectively. All samples are characterized by high abundances in Al_2O_3, LREEs, and LILEs, but depleted in HFSEs. Together with high $Mg^{\#}$ ratios and low K/tholeiite to calc-alkaline series, these features indicated that basalt to andesite was likely derived from relatively low degree partial melting of the subduction-fluid related mantle in the spinel phase. And dacite was mainly from the partial melting of crust, then affected by mantle. All samples barely went through fractional crystallization process with the slight Eu anomaly. Compared with the contemporary basalt in NCB, rocks in BAB have a complex composition of zircon and a more positive ε_{Hf} (t) value (−6.6–6.4), indicating that they had different magma sources of rocks. Though with different basements, NCB and BAB have become an integrated whole before 278 Ma. Therefore, it could be concluded that NCB and BAB belonged to the active continental margin and the PAO had not closed yet until late Permian and then it disappeared gradually and the CAOB developed into a condition of syn-post collision.

Key words: Permian, volcanic rocks, Bilutu, Bainaimiao Arc Belt, North China Block, Central Asian Orogenic Belt

Citation: Wang et al., 2019. Permian Tectonic Evolution in the Middle Part of Central Asian Orogenic Belt: Evidence from Newly Identified Volcanic Rocks in the Bilutu Area, Inner Mongolia. Acta Geologica Sinica (English Edition), 93(5): 1281–1299. DOI: 10.1111/1755-6724.14361

1 Introduction

Developing between the Siberian Block (SB) and North China Block (NCB) through accretion of island arcs, ophiolites and microcontinents in Paleo-Asian Ocean (PAO) (Jian et al., 2008,2010; Xiao et al., 2010), the Central Asian Orogenic Belt (CAOB) is considered to be the most important and the longest site of crustal formation during Phanerozoic on the earth (Sengör et al., 1993; Jahn et al., 2000; Xiao et al., 2003; Windley et al., 2007; Wilde, 2015). The accepted terminal suture between the Siberian Block (SB) and North China Block (NCB) is Solonker suture zone which extends from Solon Obo to Linxi in Inner Mongolia and may extend to Changchun and Yanji area (Li et al., 2006; Wu et al., 2007; Lin et al., 2008; Eizenhöfer et al., 2014; Li et al., 2014; Zhang H S et al., 2018). However, the timing of the final closure and the evolution in late Paleozoic is still controversial. Some researchers proposed that the final closure of PAO was during the middle-Late Devonian to Early Carboniferous, when there was a limit intra-continental ocean basin or rift since early Permian which closed in early Mesozoic (Zhang et al., 2008; Xu et al., 2013; Zhao et al., 2013; Chu et al., 2014; Zhang J R et al., 2018). Whereas others suggested that the PAO existed during the whole Paleozoic and closed in late Permian-early Triassic (Xiao et al., 2010, 2015; Li et al., 2013; Chen et al., 2014; Chen et al., 2016; Eizenhöfer and Zhao, 2018; Guan et al., 2018;). One key to the question is to figure out the tectonic setting in Permian, that is, is it an extension or a compression setting. Therefore, it is necessary to carry out extensive investigations on various lithologies from the CAOB, especially on igneous rocks that are widespread in the belt.

The NCB and Bainaimiao Arc Belt (BAB, also named Southern Orogen by some researchers) are in the middle part of CAOB. The two units are separated by an E-W trend fault, the Chifeng-Bayan obo fault zone (Fig. 1) (Wang and Liu, 1986; Hu et al., 1990; BGMRIM, 1991; Jong et al., 2006). The northern border of the BAB is the Xar Moron fault, where the Ondor Sum subduction-accretion complex in the north (Tang and Yan, 1993; Li et

* Corresponding author. E-mail: dxj@jlu.edu.cn

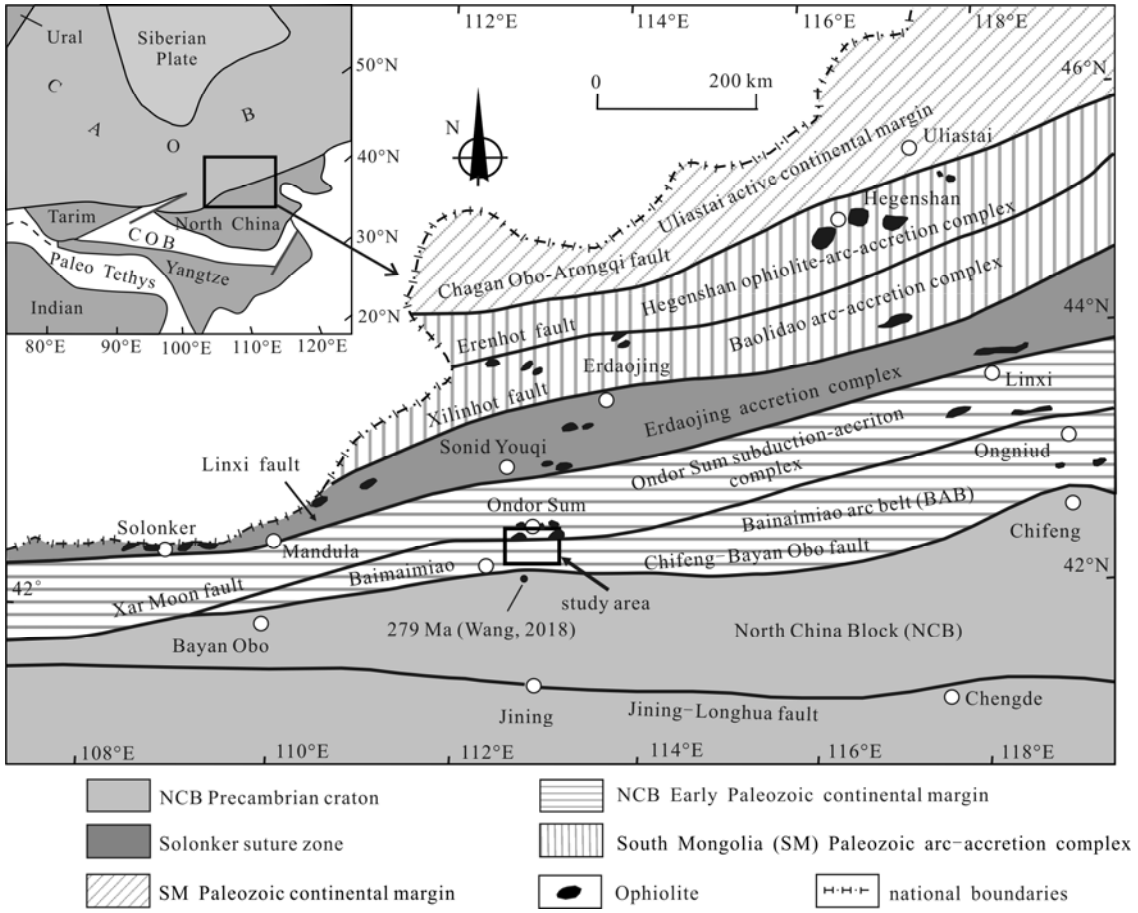

Fig. 1. Simplified sketch map of the Central Asia Orogenic Belt (modified from Jahn, 2000) and a regional tectonic sketch of middle Inner Mongolia (modified from Xiao et al., 2003).

al., 2012). The BAB is mainly composed of low grade metasedimentary, early Paleozoic igneous rocks, some Permian intrusive rocks and stratum (Liu et al., 2014). The relationship of most geologic units is not clear, especially in the exposed volcanic rocks, so it is difficult to determine their accurate age. Recently, many researchers have focused on the volcanic rocks in BAB and concluded that they may form in early Paleozoic (411–518 Ma) (Zhang et al., 2014). However, some Permian volcanic rocks have been identified from this area which was previously mapped and regarded as the early Paleozoic formation, Baimaimiao Group. Furthermore, it still uncertain that whether the volcanic rocks in BAB are identical with those in NCB. Therefore, geochronological and geochemical data for the newly-identified volcanic rocks were presented in this paper with the aim to reveal their petrogenesis and tectonic implication, which is of great significance to explore the late-Paleozoic tectonic evolution in CAOB.

2 Geological Background

The BAB in central Inner Mongolia extends about 1300 km (Tang, 1990; Zhang et al.,2014) and has been deformed and destroyed seriously by subsequent magmatic-tectonic activities. The study area is near Bilutu and is located within the middle BAB and bounded by the Ondor Sum fault, as a part of the Xar Moron fault (Fig. 2). This area records abundant intrusive rocks from Cambrian to Mesozoic and contains late Paleozoic sediments of Silurian Xibiehe formation, Carboniferous Benbatu and Amushan formation, Permian Sanmianjing formation. The volcanic rocks distribute in this area are limited and only outcrop Miocene basalt, Jurassic Manitu formation and some Permian volcanic rocks that were just separated from the Bainaimiao Group. Considering its complex contact relations with adjacent units and the incomplete sequence restricted by faults, this study did not classify them into a contemporary unit, such as Elitu or Suji formation. Besides, early Paleozoic formation, Ondor Sum group, and Bainaimiao group also exposure in this area. The former is mainly composed of meta-basalts, meta-gabbro, quartzite, and quartz schist, while the latter is composed of greenschist-facies meta-volcanic-sedimentary. There is also a small region of ophiolite in the middle area (Liu et al., 2003). Excluding minor Permian layer and Miocene basalt uncomfortably overlaid on the previous units, almost all the units have been intruded and transformed by Permian granitoid and faults.

3 Samples

Two geological sections PM2 and PM12 in this study area have been plotted after the fieldwork. There are

various rock types in PM2, such as sandstone, basic-intermediate volcanic rocks, and granites. The Permian volcanic rocks are fault contact with Benbatu and Jiujuzi formation (Fig. 3a). While PM12 exhibited a series of intermediate-acid volcanic rocks from andesite to rhyolite which exposed in a stable attitude relatively, and they cover Sanmianjing formation comfortably (Fig. 3b). All the rocks have been deformed to some degrees that cleavage and alteration can be observed frequently (Figs. 4a, 4d), faults also exist in both sections. The samples used in this study were mainly collected from these two sections.

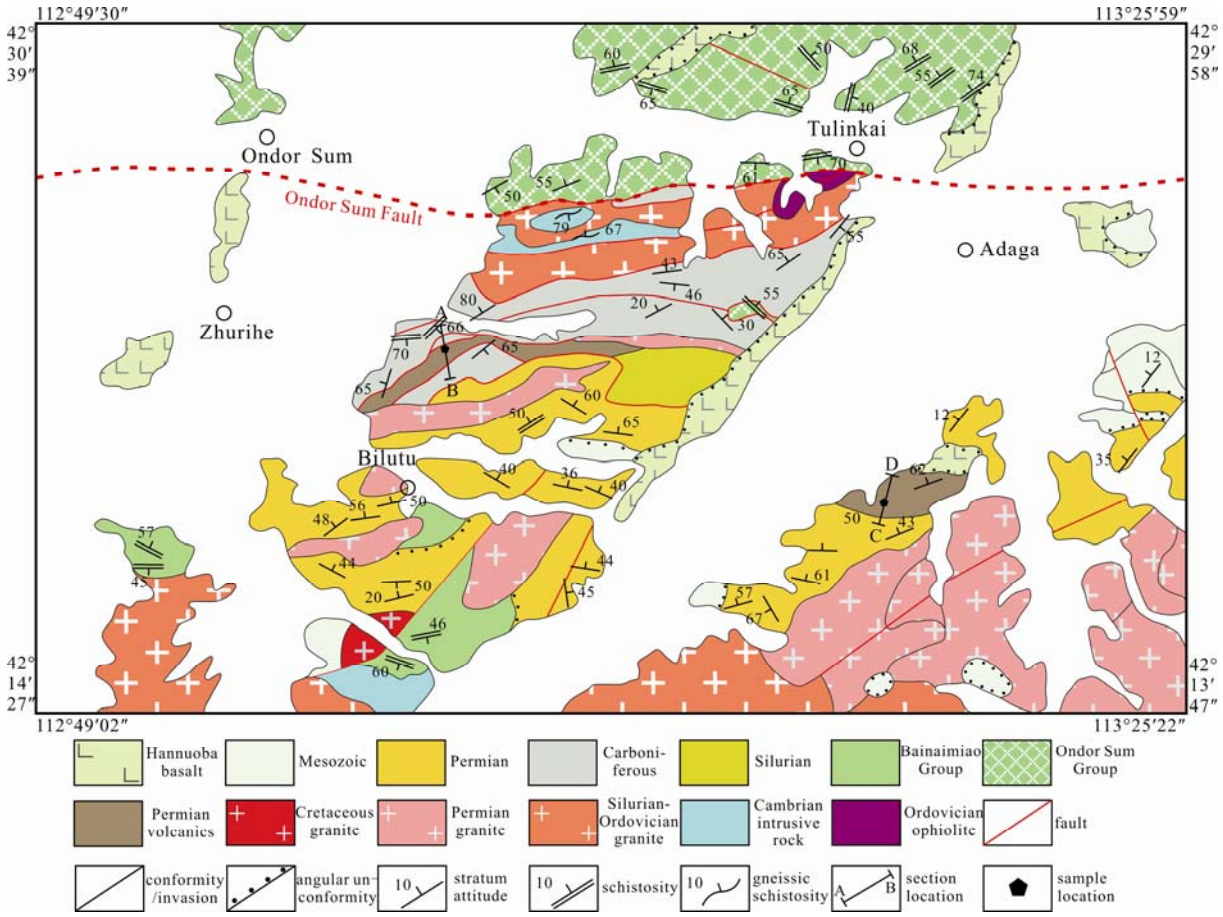

Fig. 2. Simplified geological map of the Bilutu area. Modified from the geological map (scale, 1:250 000) of Sonid Right Banner region.

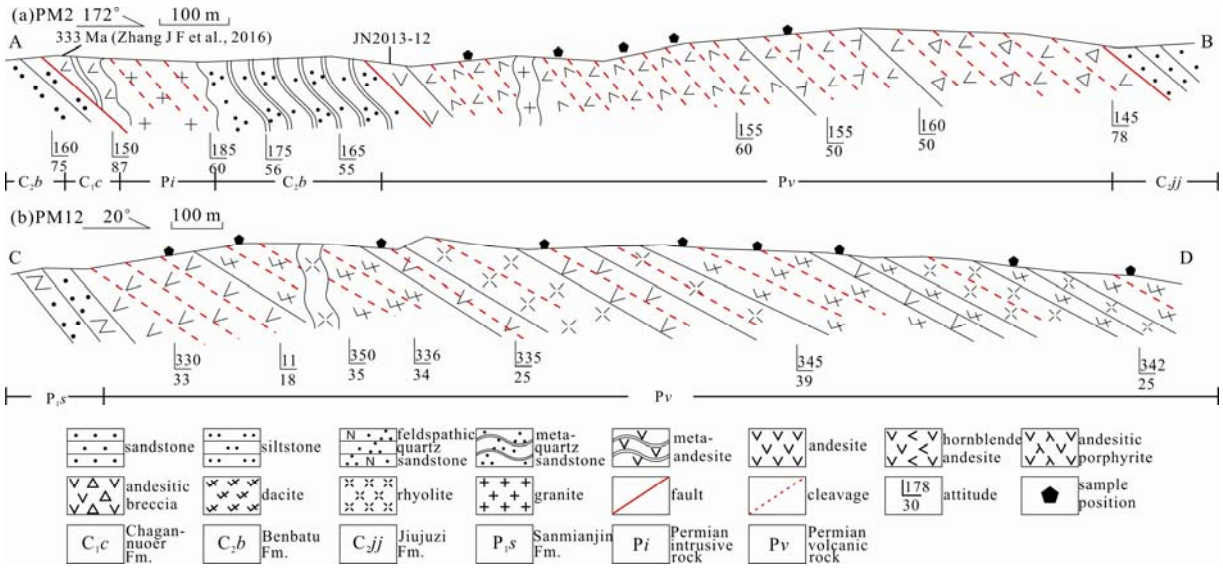

Fig. 3. Geological sections in the study area.

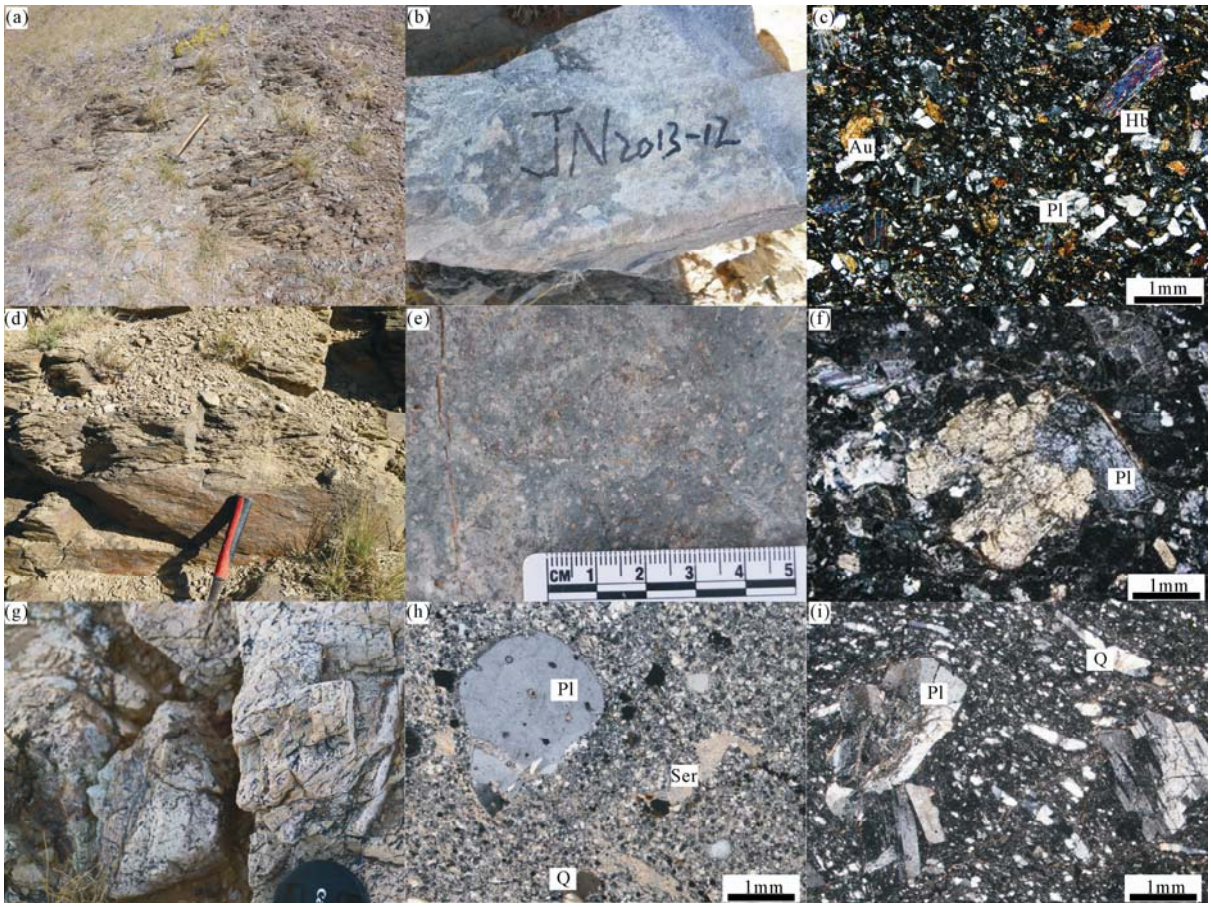

Fig. 4. Photos of outcrops and microphotographs of representative rock samples.
(a) basaltic andesite in PM2; (b, c) specimen photo and cross-polarized light photo of sample JN2013-12; (d) andesite in PM12; (e, f) specimen photo and cross-polarized light photo of sample TW0111; (g) rhyolite in PM12; (h) cross-polarized light photo of rhyolite; (i) cross-polarized light photo of dacite. Au = Augite; Hb = Hornblende; Pl = Plagioclase; Q = Quartz; Ser = Sericite.

PM2: Basic-intermediate volcanic rock (group 1)

This suit is mainly composed of andesite (3 samples), basaltic andesite (2 samples), and andesite tuff (JN2013-12). Except that sample JN2013-12 is of crystal-tuff texture, the others are porphyritic, and most phenocrysts are idiomorphic (Fig. 4b). All the samples have a similar main mineral composition with plagioclase (30–35%), augite (10–15%), hornblende (5%) and minor quartz (3%) (Fig. 4c). All of them were collected for geochemical analyses and sample JN2013-12 (113°02′14.84″E, 42°23′02.86″N) was also used for U-Pb dating.

PM12: Intermediate-acid volcanic rocks

Andesite, dacite, and rhyolite appear in this section, they had almost experienced alteration and some minerals were arranged directionally. Sericitization and kaolinization could be observed clearly in the matrix in some rocks. Two andesite samples and six dacite samples were collected for geochemical analyses, and another andesite sample TW0111 (113°16′18.31″E, 42°18′53.06″N) was used for U-Pb date.

Andesite (group 2): the samples are dark gray, porphyritic and massive structure (Fig. 4e), and phenocryst assemblages consisted of plagioclase (15%–20%), K-feldspar (5%), quartz (3%) and minor dark minerals (5%) which had lost their initial shape (Fig. 4f).

Rhyolite: The sample has an off-white color (Fig. 4g), is porphyritic, and contains phenocrysts of plagioclase (15%–20%), quartz (10%–15), and minor muscovite and plagioclase in a groundmass of feldspar and quartz. Felsitic texture and sericite (15%–20%) can be observed in some samples (Fig. 4h).

Dacite (group 3): The sample is grey, porphyritic, and contains phenocrysts of plagioclase (30% of the rock mass), hornblende (5%), and minor quartz in a very fine-grained groundmass of feldspar and quartz (Fig. 4i). Intertexture structure and amygdaloidal structure can be observed in some samples.

4 Analytical Methods

4.1 Zircon U-Pb dating

Zircons were separated from whole-rock samples with conventional magnetic and heavy liquid techniques and purified by hand-picking under a binocular microscope at the Langfang Regional Geological Survey, Hebei Province, China. Cathodoluminescence (CL) images were obtained to identify the internal textures.

Sample (JN2013-12) was analyzed at the MRL Key Laboratory of Metallogeny and Mineral Assessment, Institute of Mineral Resource, Chinese Academy of

Fig. 5. Cathodoluminescence (CL) images and test spots of representative zircons in this study.

Geological Sciences, Beijing, China, and sample (TW0111) was analyzed in the Isotopic Laboratory of Tianjin Geological Survey Center, Tianjin, China. Both samples employed a Neptune inductively coupled plasma-mass spectrometer (ICP-MS) and laser ablation (LA) with GJ-1 standard zircon for external age calibration. Details of the parameters are given by Hou et al. (2009) and the correction for the common Pb contribution followed Andersen (2002). The weighted average data of the zircon age and Concordia plots were made using ISOPLOT 3.0 (Ludwig, 2003) given at the 95% confidence level.

4.2 Major and trace elements

Samples in Group 1 were analyzed at the ASL Minerals -ALS Chemex laboratory in Guangzhou, China, samples in group 2 and 3 at Isotopic Laboratory of Tianjin Geological Survey Center, Tianjin, China. All fresh samples were crushed and ground to 200 mesh after the removal of alteration of the surface. Major elements were measured using X-ray fluorescence (XRF) and the trace element compositions were determined by ICP-MS. The analytical precision and accuracy values are better than 5% for the major elements and better than 10% for the trace elements.

4.3 Zircon Hf isotopes

Only sample JN2013-12 was used for Hf isotopes data. In situ zircon Hf isotope analyses were conducted using a New Wave UP 213 LA system attached to a Neptune multicollector ICP-MS (MC-ICP-Ms) at the MRL Key Laboratory of Metallogeny and Mineral Assessment, Institute of Mineral Resources, Chinese Academy of Geological Sciences, Beijing, China. The detailed analytical procedure and data acquisition were described by Wu et al. (2006) and Hou et al. (2007).

5 Results

5.1 Zircon U-Pb data and Hf-isotope compositions

Zircons taken from two representative samples were separated for U-Pb isotopic dating. All the zircons are mostly euhedral to subhedral, stubby to elongate prisms, with common internal oscillatory zoning in CL images (Fig. 5). Besides, the zircons are mostly 60–200 μm long and have the length/width ratios of ca. 1.2–4.0. Combined with their high Th/U ratios (0.36–5.38), it could be concluded that they have an igneous origin (Koschek 1993; Belousova et al. 2002). The results are listed in table 1.

5.1.1 Sample JN2013-12

20 zircon grains were analyzed for U-Pb isotopic compositions. Except for the zircon grains (1, 2, 17), others yielded concordance of 95–99%. There were 8 zircon grains aged from 272 to 284 Ma with a weighted mean $^{206}Pb/^{238}U$ age of 278.2±4.1 Ma (MSWD=0.29, n=8). This age represents the crystallization age, and the older ages (304–421 Ma, 1363–2458 Ma) represent inheritance formed during earlier magmatic events (Figs. 6a, 6b). The eight younger zircons chosen for in-situ Hf-isotope analysis were relatively smaller and only four of them showed available data. They have Hf isotopic compositions with $\varepsilon_{Hf}(t)$ values of −6.6–6.4 and $^{176}Hf/^{177}Hf$ ratios of 0.282413–0.28779 (Fig. 7), yielding single-stage (T_{DM1}) and two-stage (T_{DM2}) Hf model ages from1243 to 757 Ma and from 2315 to 1148 Ma respectively (Table 2).

5.1.2 Sample TW0111

A total of 34 analyses of zircons from sample TW0111 yielded $^{206}Pb/^{238}U$ ages from 256 to 2412 Ma except for discordant grains (7, 11, 18, 24, 31, 32). Four youngest zircons had a weighted mean $^{206}Pb/^{238}U$ age of 258.3±3.0 Ma (MSWD=3.1, n=4; Figs. 6c, 6d) which represented the crystallization age. In addition, the remaining zircons yielded older ages of 271.0±1.0 Ma (n=4), 399.4±2.8 Ma (n=8), 420.6±0.9Ma (n=8), 441.3±1.4 Ma (n=3), 499.4 Ma, 881.6 Ma, 1028.1 Ma,1804.1Ma, 2412.8 Ma, which were interpreted as due to inheritance.

5.2 Major and trace elements

The major and trace element compositions of 14 representative samples from the Bilutu area are listed in Table 3.

Group 1 samples from PM2 contain poor concentrations of SiO_2 (46.82–52.62 wt%) and Na_2O+K_2O (3.15–5.05 wt%). They are plotted into the field of basalt, trachy basalt and basaltic andesite in the total alkali (K_2O +

Table 1 LA-ICP-MS U-Pb dating results of the Permian volcanic rocks

Grain	Content (ppm)				ratios						Age (Ma)					
Spot	Pb	Th	U	Th/U	$^{207}Pb/^{206}Pb$	σ	$^{207}Pb/^{235}U$	σ	$^{206}Pb/238U$	σ	$^{207}Pb/^{206}Pb$	σ	$^{207}Pb/^{235}U$	σ	$^{206}Pb/^{238}U$	σ
JN2013-12																
3	8	228	76	2.99	0.05155	0.00662	0.31770	0.03935	0.04473	0.00126	265	335	280	30	282	8
4	7	200	75	2.69	0.05176	0.00490	0.31584	0.03060	0.04399	0.00124	276	218	279	24	278	8
5	16	59	13	4.57	0.16967	0.00489	10.78579	0.29411	0.46438	0.00790	2555	48	2505	25	2459	35
6	62	205	147	1.40	0.09516	0.00272	3.10195	0.08323	0.23561	0.00388	1531	54	1433	21	1364	20
7	29	80	47	1.71	0.11609	0.00325	4.96220	0.13504	0.31053	0.00510	1898	46	1813	23	1743	25
8	6	157	51	3.10	0.05607	0.00546	0.36509	0.03178	0.04840	0.00120	454	212	316	24	305	7
9	10	251	103	2.44	0.05181	0.00357	0.32105	0.02135	0.04451	0.00097	276	159	283	16	281	6
10	15	241	110	0.62	0.05548	0.00231	0.51924	0.02110	0.06749	0.00100	432	88	425	14	421	6
11	13	234	123	0.25	0.05526	0.00376	0.41049	0.02893	0.05361	0.00103	433	154	349	21	337	6
12	11	225	137	0.98	0.05187	0.00305	0.31265	0.01691	0.04412	0.00072	280	135	276	13	278	4
13	16	436	164	0.91	0.05411	0.00301	0.33133	0.01669	0.04426	0.00111	376	119	291	13	279	7
14	12	344	136	0.16	0.05220	0.00510	0.30855	0.02871	0.04312	0.00100	295	224	273	22	272	6
15	20	473	186	1.07	0.05436	0.00397	0.38032	0.03154	0.05059	0.00141	387	165	327	23	318	9
16	104	180	178	2.33	0.11440	0.00271	5.29593	0.14117	0.33255	0.00497	1872	47	1868	23	1851	24
18	17	754	140	5.39	0.05177	0.00541	0.32285	0.03494	0.04512	0.00154	276	241	284	27	284	9
19	16	387	181	2.13	0.05224	0.00272	0.31903	0.01735	0.04395	0.00065	295	119	281	13	277	4
20	147	391	174	2.25	0.15663	0.00316	9.05585	0.18097	0.41811	0.00533	2420	34	2344	18	2252	24
TW0111																
1	42	210	198	1.06	0.05189	0.00189	0.44815	0.01670	0.06312	0.00026	280	83	376	12	395	2
2	24	171	210	0.81	0.05025	0.00245	0.29446	0.01444	0.04283	0.00025	206	108	262	11	270	2
3	66	278	369	0.75	0.05567	0.00122	0.51571	0.01289	0.06742	0.00025	439	48	422	9	421	2
4	35	116	229	0.51	0.05286	0.00256	0.51489	0.02460	0.07116	0.00038	324	109	422	16	443	2
5	36	145	220	0.66	0.05196	0.00164	0.43843	0.01414	0.06162	0.00018	283	72	369	10	385	1
6	44	191	228	0.84	0.05459	0.00189	0.48193	0.01753	0.06436	0.00022	394	78	399	12	402	1
8	55	398	388	1.03	0.05469	0.00131	0.30786	0.00783	0.04106	0.00016	398	54	273	6	259	1
9	44	166	280	0.59	0.05475	0.00165	0.50637	0.01558	0.06749	0.00022	467	73	416	11	421	1
10	34	129	213	0.61	0.05244	0.00207	0.45355	0.01847	0.06303	0.00029	306	89	380	13	394	2
12	77	561	665	0.84	0.05107	0.00106	0.30065	0.00661	0.04293	0.00013	243	53	267	5	271	1
13	65	322	731	0.44	0.05123	0.00065	0.28715	0.00389	0.04095	0.00018	250	30	256	3	259	1
14	25	71	194	0.37	0.05247	0.00228	0.45925	0.02131	0.06363	0.00030	306	128	384	15	398	2
15	70	339	327	1.04	0.05255	0.00095	0.46278	0.00896	0.06424	0.00024	309	8	386	6	401	1
16	37	150	207	0.73	0.05189	0.00158	0.45322	0.01377	0.06379	0.00024	280	70	380	10	399	1
17	99	69	139	0.50	0.10713	0.00091	4.74836	0.05573	0.32298	0.00152	1751	15	1776	10	1804	7
19	93	434	451	0.96	0.05383	0.00215	0.48308	0.02547	0.06460	0.00032	365	89	400	17	404	2
20	59	243	307	0.79	0.05510	0.00088	0.50986	0.00870	0.06722	0.00018	417	31	418	6	419	1
21	322	164	304	0.54	0.15684	0.00078	9.80466	0.08338	0.45396	0.00265	2422	9	2417	8	2413	12
22	34	123	205	0.60	0.05450	0.00095	0.50438	0.00871	0.06735	0.00026	391	39	415	6	420	2
23	21	110	211	0.52	0.05106	0.00155	0.30530	0.00954	0.04323	0.00021	243	75	271	7	273	1
25	37	229	325	0.71	0.05315	0.00116	0.31554	0.00696	0.04303	0.00016	345	50	278	5	272	1
26	73	339	356	0.95	0.05641	0.00075	0.52493	0.00699	0.06745	0.00021	478	30	428	5	421	1
27	86	630	701	0.90	0.05200	0.00056	0.29600	0.00356	0.04127	0.00022	283	24	263	3	261	1
28	44	179	256	0.70	0.05507	0.00088	0.51256	0.00849	0.06747	0.00030	417	31	420	6	421	2
29	41	247	249	0.99	0.05448	0.00218	0.38521	0.01538	0.05125	0.00016	391	91	331	11	322	1
30	142	119	177	0.67	0.11164	0.00058	4.97614	0.03170	0.32294	0.00105	1828	9	1815	6	1804	5
33	97	113	303	0.37	0.07232	0.00060	1.72908	0.02013	0.17290	0.00100	994	12	1019	8	1028	6
34	60	215	335	0.64	0.05912	0.00088	0.57711	0.00849	0.07076	0.00015	572	36	463	5	441	1
35	49	231	248	0.93	0.05333	0.00077	0.49642	0.00723	0.06750	0.00021	343	33	409	5	421	1
36	87	371	490	0.76	0.05724	0.00049	0.53336	0.00465	0.06755	0.00020	502	19	434	3	421	1
37	74	343	185	1.85	0.05706	0.00084	0.63313	0.00928	0.08054	0.00033	494	33	498	6	499	2
38	67	320	260	1.23	0.05842	0.00135	0.57160	0.01320	0.07093	0.00022	546	50	459	9	442	1
39	30	128	182	0.70	0.05406	0.00224	0.47954	0.01982	0.06420	0.00021	372	94	398	14	401	1
40	48	389	385	1.01	0.05037	0.00212	0.28127	0.01147	0.04054	0.00015	213	92	252	9	256	1

Table 2 Hf isotope results of zircons from the Permian volcanic rocks

Spot	$^{176}Yb/^{177}Hf$	σ	$^{176}Lu/^{177}Hf$	σ	$^{176}Hf/^{177}Hf$	σ	$\varepsilon_{Hf}(0)$	$\varepsilon_{Hf}(t)$	σ	Age (Ma)	T_{DM1}(Ma)	T_{DM2}(Ma)	$f_{Lu/Hf}$
JN2013-12													
4	0.297091	0.014173	0.008336	0.000274	0.282823	0.000536	1.8	6.4	18.97	278	757	1148	−0.75
12	0.163045	0.007097	0.003485	0.000148	0.282431	0.000044	−12.1	-6.6	1.57	276	1243	2315	−0.90
14	0.082484	0.000985	0.002202	0.000041	0.282712	0.000022	−2.1	3.5	0.77	276	791	1408	−0.93
19	0.139205	0.002358	0.003367	0.000047	0.282741	0.000051	−1.1	4.4	1.80	269	774	1329	−0.90

Na_2O) vs. silica (SiO_2) classification diagram (Fig. 8a), most of which fall into the field of basaltic andesite. Moreover, those rocks had low K_2O contents, indicative of low-K to tholeiiteto calc-alkaline series (Fig. 8b) and had relatively high contents of TiO_2, Al_2O_3, FeO^T, MgO and CaO. All these rocks showed parallel rare earth element (REE) pattern in the chondrite normalized diagrams (ΣREE=176.7–382.1 ppm, Fig. 9a), with enrichment of light rare earth elements (LREE, $(La/Yb)_N$=15.20–37.44), nearly flatten heavy rare earth elements (HREE, (Gd/Yb)

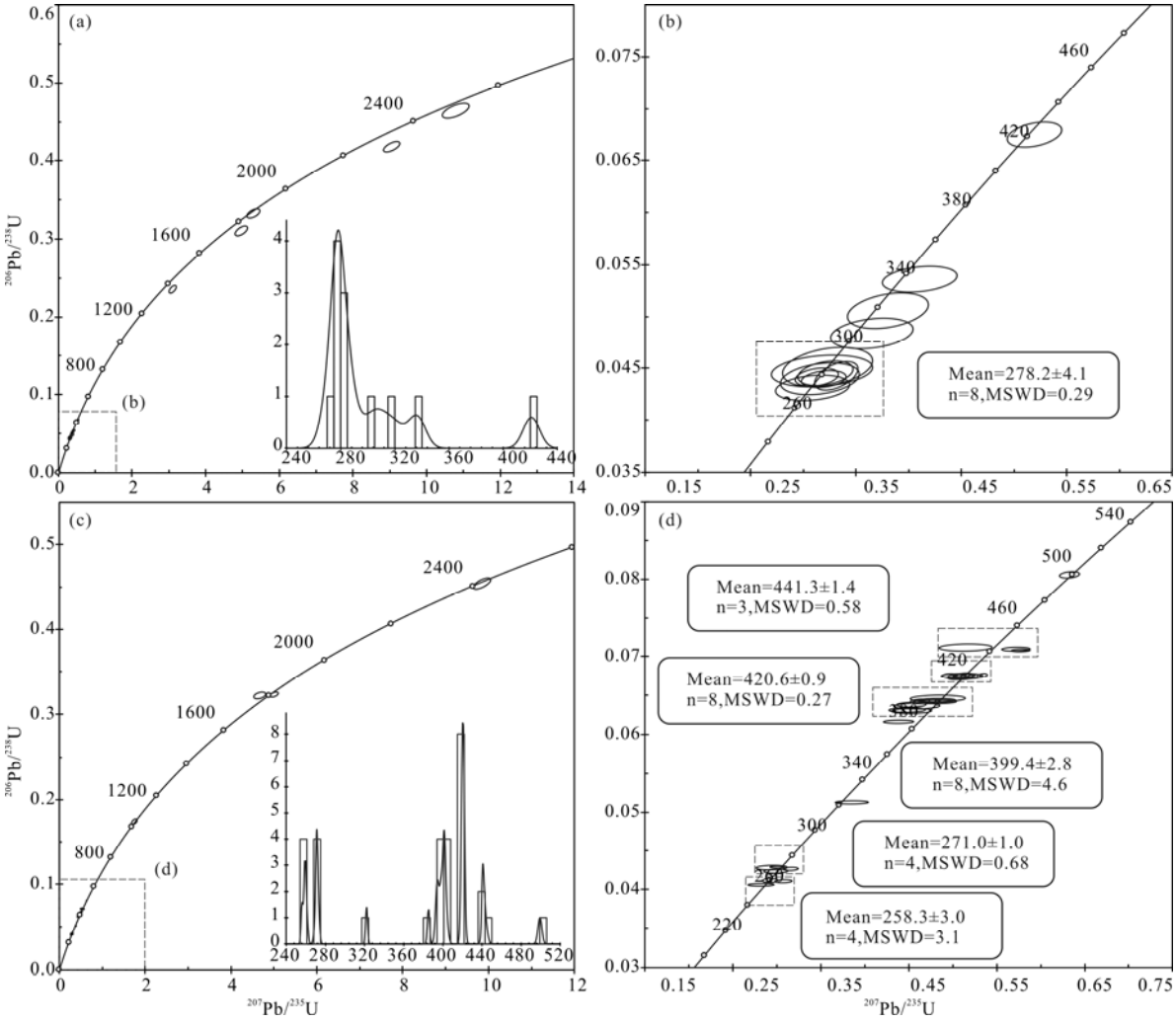

Fig. 6. Zircon U-Pb Concordia diagrams and density histograms from the dated samples.

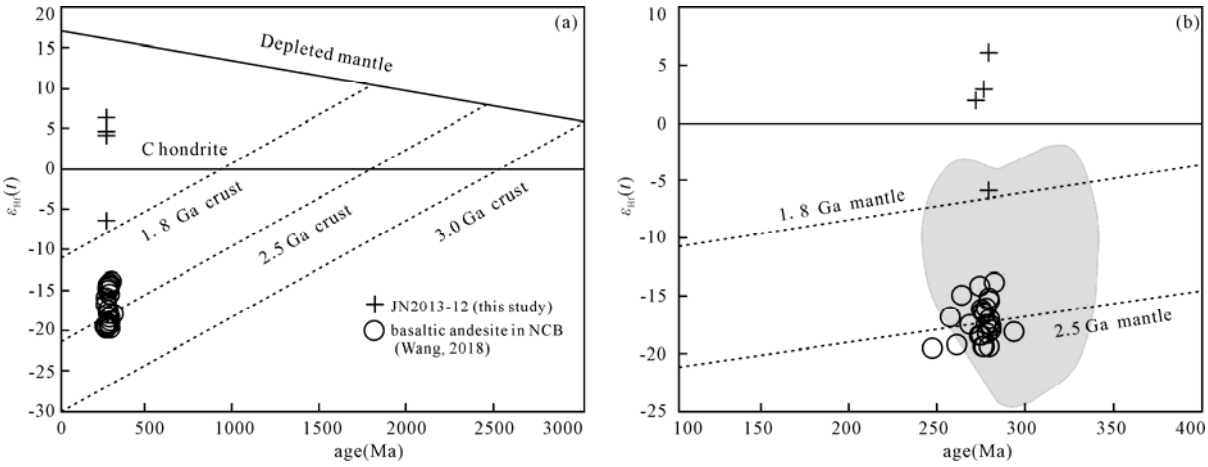

Fig. 7. Correlations between $\varepsilon_{Hf}(t)$ values and zircon ages for sample JN2013-12.
Data of circular spots and shaded area are referred from references (Wang, 2018; Zhang S H, et al., 2016) respectively.

$_N$=2.23–4.08) and slight negative Eu anomalies (δEu=0.82–0.92). In the primitive mantle normalized trace-element diagram (Fig. 9b), the samples showed significant enrichment in the large ion lithophile elements (LILE; e.g. Cs, Sr, and Eu) as well as depletion in the high field strength elements (HFSE; e.g. Nb, Ta, and Ti).

Group 2 and group 3 from PM12 yielded higher SiO_2 (56.72–68.98 wt%), K_2O and MgO but lower Fe_2O_3, CaO and TiO_2 contents in comparison with the samples in PM2. In the total alkali (K_2O+Na_2O) vs. silica (SiO_2)

classification diagram (Fig. 8a), these rocks were plotted within the andesite and dacite field. In K_2O vs. silica (SiO_2) classification diagram (Fig. 8b), almost all samples fall into calc-alkaline to high-K calc-alkaline series. The A/CNK values are 0.79–2.74 (mean value=1.47), which were of peraluminous compositions.

Two groups were all featured by parallel chondrite normalized REE patterns (ΣREE=111.36–183.30 ppm, 123.18–174.99 ppm), enrichment of LREEs ($(La/Yb)_N$=7.36–8.37, 7.24–11.79), negligible differentiation of HREEs ($(Gd/Yb)_N$=1.47–1.85, 1.26–1.83) and moderate negative Eu anomalies (δEu=0.86–0.88, 0.77–0.91) (Figs. 9c, 9e). Enrichment in LILEs (e.g. Cs and K) together with depletion in HFSEs (Nb, Ta, and Ti) were observed in the primitive mantle normalized trace-element diagram (Figs. 9d, 9f).

6 Discussions

6.1 Permian volcanism in BAB

In this study, some Permian volcanic rocks were found among the units, which were considered to be formed in

Table 3 Major and trace element compositions of the Permian volcanic rocks

Number	JN2013-12	P2b29-1	P2b29-2	P2b30-1	P2b32-2	P2b33-1	PM12-2-3
Major element oxides (wt%)							
SiO_2	50.40	46.82	48.69	52.62	47.44	52.39	62.72
TiO_2	0.64	0.55	0.65	0.68	0.84	0.70	0.55
Al_2O_3	16.70	14.73	15.78	15.90	15.56	17.33	15.28
Fe_2O_3	8.76	6.49	8.37	5.35	4.34	6.26	2.37
FeO		0.88	1.78	4.07	5.39	2.49	3.47
MnO	0.12	0.092	0.16	0.10	0.15	0.15	0.13
MgO	5.39	1.56	3.77	5.27	7.45	3.44	3.15
CaO	9.66	14.86	10.48	9.08	11.80	9.95	2.25
Na_2O	4.02	4.92	4.81	3.57	2.71	2.91	3.71
K_2O	0.28	0.13	0.90	0.17	0.52	0.24	1.91
P_2O_5	0.21	0.30	0.22	0.31	0.35	0.44	0.15
LOI	3.53	8.48	4.91	2.34	2.76	3.32	3.93
Total	99.71	99.81	99.71	99.46	99.31	99.62	99.62
H_2O^+	-	1.56	2.17	2.16	2.14	2.18	-
CO_2	-	5.632	1.866	0.042	0.414	0.948	-
$Mg^{\#}$	56.56	30.66	43.54	53.05	60.42	44.65	51.71
Trace elements (ppm)							
La	38.9	51.5	37.1	49.5	46.0	88.3	23.4
Ce	72.0	93.5	66.6	84.4	89.2	157.0	45.3
Pr	8.34	10.70	7.70	9.77	10.8	17.80	5.40
Nd	30.8	39.9	30.0	37.3	43.1	66.1	21.2
Sm	5.69	7.10	5.68	6.87	8.46	11.30	4.22
Eu	1.58	1.69	1.44	1.74	2.17	2.69	1.11
Gd	4.56	4.90	3.93	4.83	5.79	8.04	3.79
Tb	0.54	0.67	0.60	0.70	0.86	1.02	0.60
Dy	3.14	2.98	2.82	3.44	4.38	4.00	3.57
Ho	0.57	0.56	0.54	0.64	0.84	0.70	0.76
Er	1.69	1.56	1.49	1.82	2.23	1.85	2.18
Tm	0.22	0.21	0.20	0.26	0.30	0.23	0.33
Yb	1.36	1.39	1.32	1.75	2.04	1.59	2.18
Lu	0.21	0.20	0.20	0.27	0.32	0.23	0.33
Y	15.6	18.3	17.1	17.7	22.1	21.2	19.1
ΣREE	185.20	235.16	176.72	220.99	238.59	382.05	133.47
La_N/Yb_N	19.28	24.98	18.95	19.07	15.20	37.44	7.24
δEu	0.92	0.83	0.88	0.88	0.90	0.82	0.83
Cs	0.15	0.22	0.14	0.17	0.31	0.20	1.42
Rb	5.20	3.41	2.53	2.83	7.68	5.17	37.5
Sr	686	619	784	970	687	1040	183.0
Ba	223	209	321	225	711	226	540
Ga	17.8	-	-	-	-	-	14.6
Nb	4.20	3.02	2.70	4.12	3.92	5.09	7.05
Ta	0.20	0.19	0.19	0.25	0.24	0.32	0.46
Zr	103.0	76.4	64.2	102.0	102.0	129.0	106.0
Hf	2.70	2.06	1.95	2.97	3.04	3.35	3.60
Th	11.10	9.82	9.97	10.20	11.70	16.20	9.71
V	299	254	314	284	346	258	141
Cr	110.0	87.4	184.0	151.0	222.0	20.7	12.9
Co	-	26.3	44.9	29.1	42.9	26.3	17.0
Ni	-	25.5	49.3	33.3	42.6	17.1	6.2
Li	-	-	-	-	-	-	9.21
Sc	33.0	26.9	43.8	33.8	57.1	25.8	20.3
U	2.91	2.42	1.45	1.65	2.66	3.51	1.77
Pb	-	-	-	-	-	-	15.10
Zn	-	-	-	-	-	-	84.2
Cu	-	-	-	-	-	-	62.0

Continued Table 3

Number	PM12-3-1	P12-4-2	P12-6-1	P12-10-1	P12-13-1	P12-14-1	P12-20-1
Major element oxides (wt%)							
SiO_2	64.52	58.51	66.30	56.72	65.75	64.28	68.98
TiO_2	0.43	0.57	0.50	0.59	0.61	0.48	0.52
Al_2O_3	16.61	16.98	15.20	15.53	16.21	15.5	14.51
Fe_2O_3	3.74	7.45	2.96	4.68	3.37	3.39	2.89
FeO	0.25	1.16	1.94	3.35	1.02	1.66	1.09
MnO	0.12	0.23	0.22	0.15	0.05	0.12	0.11
MgO	1.14	4.93	3.94	4.29	1.89	2.52	2.08
CaO	1.82	0.52	0.32	3.69	0.54	2.48	1.21
Na_2O	5.49	1.43	1.98	4.75	3.09	3.78	1.95
K_2O	1.73	2.67	3.01	1.39	4.81	3.25	2.94
P_2O_5	0.20	0.26	0.14	0.17	0.26	0.17	0.14
LOI	3.94	5.16	3.29	4.31	2.29	2.20	3.47
Total	99.99	99.87	99.80	99.62	99.89	99.83	99.89
H_2O^+	-	-	-	-	-	-	-
CO_2	-	-	-	-	-	-	-
$Mg^{\#}$	37.52	54.42	61.98	51.94	47.04	50.47	51.77
Trace elements (ppm)							
La	33.4	29.8	28.2	20.1	30.6	22.1	23.9
Ce	69.4	67.9	61.1	35.3	64.3	44.6	44.7
Pr	7.35	7.49	6.31	4.77	7.09	5.08	5.36
Nd	28.0	30.8	24.4	19.3	28.1	19.6	20.8
Sm	5.08	6.51	4.83	3.89	5.47	3.80	3.97
Eu	1.24	1.72	1.26	1.06	1.48	1.10	0.96
Gd	4.34	5.51	4.27	3.36	4.65	3.46	3.51
Tb	0.60	0.83	0.67	0.52	0.71	0.52	0.56
Dy	3.19	4.38	3.93	2.92	3.90	2.94	3.29
Ho	0.66	0.88	0.83	0.61	0.82	0.62	0.71
Er	1.85	2.36	2.38	1.74	2.30	1.76	2.08
Tm	0.28	0.36	0.37	0.27	0.35	0.26	0.33
Yb	1.91	2.40	2.50	1.84	2.36	1.86	2.24
Lu	0.29	0.36	0.38	0.28	0.36	0.28	0.34
Y	17.4	22.0	21.7	15.4	20.5	15.2	18.4
ΣREE	174.99	183.30	163.13	111.36	172.99	123.18	131.15
La_N/Yb_N	11.79	8.37	7.60	7.36	8.74	8.01	7.19
δEu	0.79	0.86	0.83	0.88	0.88	0.91	0.77
Cs	1.06	2.76	2.27	0.65	2.55	1.26	2.52
Rb	33.1	51.2	51.6	14.5	86.8	61.9	74.8
Sr	374.0	69.3	53.3	431.0	142.0	457.0	55.8
Ba	460	456	813	583	1020	882	346
Ga	11.4	17.6	14.5	14.2	15.2	13.6	12.9
Nb	7.03	5.99	8.23	4.15	5.74	7.68	7.01
Ta	0.45	0.38	0.58	0.26	0.37	0.68	0.49
Zr	106.0	72.5	118.0	60.5	80.8	116.0	104.0
Hf	3.45	3.02	3.94	2.58	3.52	3.82	3.49
Th	10.20	9.29	9.84	7.98	10.80	11.80	8.69
V	91	167	107	233	136	118	119
Cr	4.00	13.6	9.7	20.2	3.9	25.3	14.5
Co	7.0	38.6	8.2	23.4	10.9	14.5	12.8
Ni	2.3	6.1	4.1	10.2	2.2	11.4	5.9
Li	1.14	37.10	11.10	10.90	8.79	11.80	9.86
Sc	7.4	21.5	14.9	25.0	16.6	15.4	15.0
U	2.86	4.56	3.30	2.25	4.96	2.53	2.87
Pb	6.53	9.74	4.58	9.69	13.70	19.10	21.60
Zn	77.5	243.0	84.3	57.0	65.1	56.6	69.3
Cu	6.8	43.0	56.3	99.7	40.0	46.9	37.6

$Mg^{\#}=100\times(MgO/40.3044)/(MgO/40.3044+Fe_2O_3^T\times0.8998/71.844)$;
Eu_N, La_N and Gd_N are chondrite-normalized Eu, La and Gd
$Eu_N\times(Sm_N\times Gd_N)^{1/2}$; $La_N/Yb_N = (La/La_N)/(Yb/Yb_N)$

Cambrian or Mesozoic previously. It's normal to have such recognition because most Permian volcanic strata exposed partially. Besides, their top and bottom were almost destroyed by thrust faults, such as PM2 and PM12 in this study, could not be observed. For this reason, the Permian volcanic strata always exposed within Cambrian and Carboniferous-Permian volcanic-sedimentary strata and appeared as a structural window in NCB (Bai, 2015) and BAB. In recent years, many types of research have been conducted in adjacent areas and new results have been obtained, which went against the existing mapping data and the former conclusion. Zhang J F et al. (2016) found Carboniferous volcanic rocks (333 Ma) in Bainaimiao group near the study area; Qing et al. (2012) and Yang et al. (2016) collected some samples from andesite and rhyolite in Bilihe goldfield, which is about 20 km east from the area of this study (Fig. 10). They got the U-Pb ages of 270 Ma and 281 Ma that were considered to

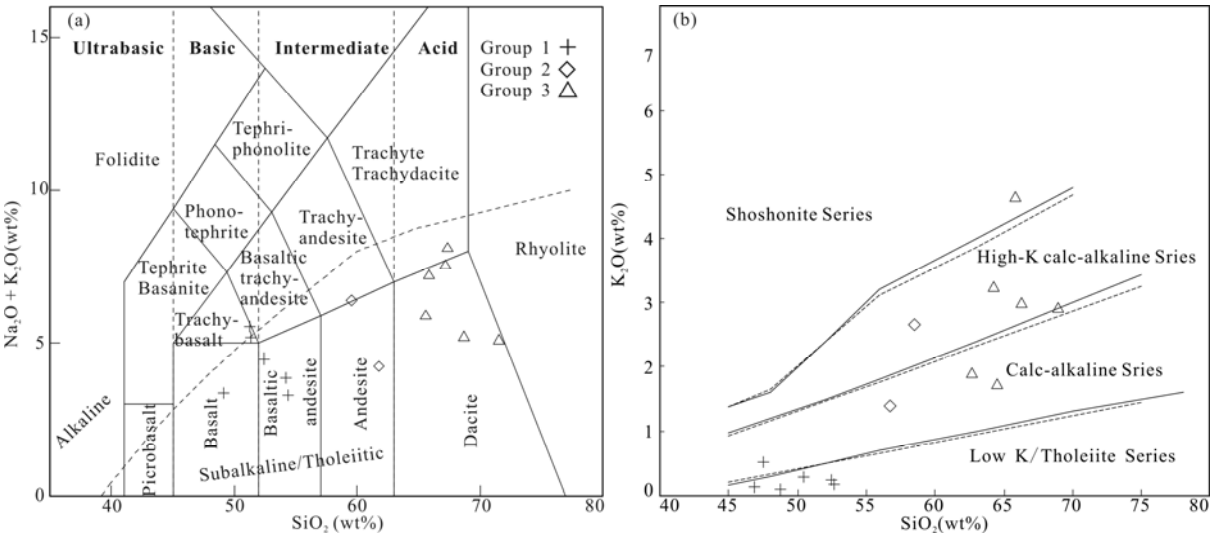

Fig. 8. Classification diagrams for the volcanic rocks.
(a) TAS diagram (after Le Bas, et al., 1986); (b) K_2O vs. SiO_2 diagram (after Peccerillo and Taylor, 1976).

be Mesozoic formation. In addition, Chu et al. (2013) presented late Permian dating (246 Ma) for meta-basic volcanic from Ondor Sum group in Tulinkai area. And the common volcanic rocks in Xianghuangqi area still lack detailed age and whether they formed in Jurassic or Permian (Zhang S H, et al. 2016; BGMRIM,1991) still remains to be studied. To sum up, some Permian volcanic rocks in BAB were mistaken as Mesozoic or were scattered within Cambrian-Ordovician formation which should be disintegrated clearly. Toughly destructed by late tectonic activities, it could also be considered that there were obvious Permian volcanic events in BAB.

6.2 Petrogenesis

6.2.1 Hydrothermal alteration effects

Under microscope, it could be observed that samples in this study have some altered minerals, with their high LOI (2.21–8.48) ratios, suggesting that they have undergone alteration in some degree, which may influence the concentrations of some incompatible elements as a result of their stronger mobility in surface alteration (Zhang et al., 2008). Ta type elements such as Ta, Ti, Zr, Hf are considered as immobile components in the whole diagenesis and metamorphism stage (Rosler and Beuge, 1983), and they are chosen as a reference to judge the mobility of other trace elements as usual (Gibson et al., 1982). Good correlation between them suggests the immobility of the other element; on the contrary, rough correlations represent they have been mobilized during the alteration. Th and Zr were chosen as abscissa to plot scatter diagrams. It shows a positive correlation with La, Nd, U in three groups of samples (Figs. 11a, 11b, 11c, 11d, 11e, 11f) and rough correlation with Ba and Sr in two groups, Rb also had a rough correlation in group 3 (Figs. 11g, 11h, 11i, 11j, 11k, 11l). These features suggest that LILEs, such as Ba and Rb, have been more or less mobilized, but the HFSEs and REEs are not obviously affected, together with the different anomalies of some samples on primitive mantle-normalized patterns (Figs. 9b, 9d, 9f). In a word, alteration processes have not significantly affected HFSEs and REEs, so they can be used to discuss the magmatic processes while LILEs should be used cautiously of some abnormal samples.

6.2.2 Origin of the volcanic rocks

Group 1 samples in PM2 display low SiO_2 (46.82–52.62 wt%) contents and relatively high $Mg^{\#}$ values (30.66–60.42), which indicates the parental magmatic sources were mainly mantle-derived. In the Nb vs. Zr diagram (Fig. 12a), group 1 are plotted in depleted mantle. The Zr/Hf (mean=35.76), Nb/Ta (mean=16.64) ratios are higher than crust (33, 11.4) and lower than primitive mantle (37, 17.8) (Sun and McDonough, 1989; Taylor and McLennan, 1985) which indicate the influence of crust. Besides, La/Nb ratio (9.26–17.35) can also be used to reveal whether there was continental contamination. This ratio is higher than primitive mantle (1.0) and crust (2.2) (Peacock et al., 1994), suggesting that the involvement of continental crust materials during raising stage is limited (Griffin et al., 2002; Zhou et al., 2018) and the addition of fluid could probably affect the La/Nb ratio (Condi, 1999).

Group 2 samples in PM12 display moderate SiO_2 (56.72–58.51 wt%), $Mg^{\#}$ values (51.94–54.42) and relatively high Pb values (9.69–9.74) compared with primitive mantle (0.185), with lower Zr/Hf ratios (mean=23.73) and moderate Nb/Ta ratios (mean=15.86) compare with primitive mantle (37,17.8) and crust (33, 11.4) (Sun and McDonough, 1989; Taylor and McLennan, 1985), suggesting a mantle-derived magma source but crust materials have played a crucial role in the process.

Group 3 samples display high SiO_2 (62.72–68.98 wt%), Pb values (6.53–21.60) and a moderate Rb/Sr ratio close to the value of crust (>0.5, Taylor and McLennan, 1985) which indicate a crust source. But relatively high $Mg^{\#}$ values (37.52–61.98) and a moderate Nb/Ta ratio (mean=14.37) between primitive mantle and curst (17.4, 11.4) (Sun and McDonough, 1989; Taylor and McLennan, 1985), suggest an influence of mantle source during the

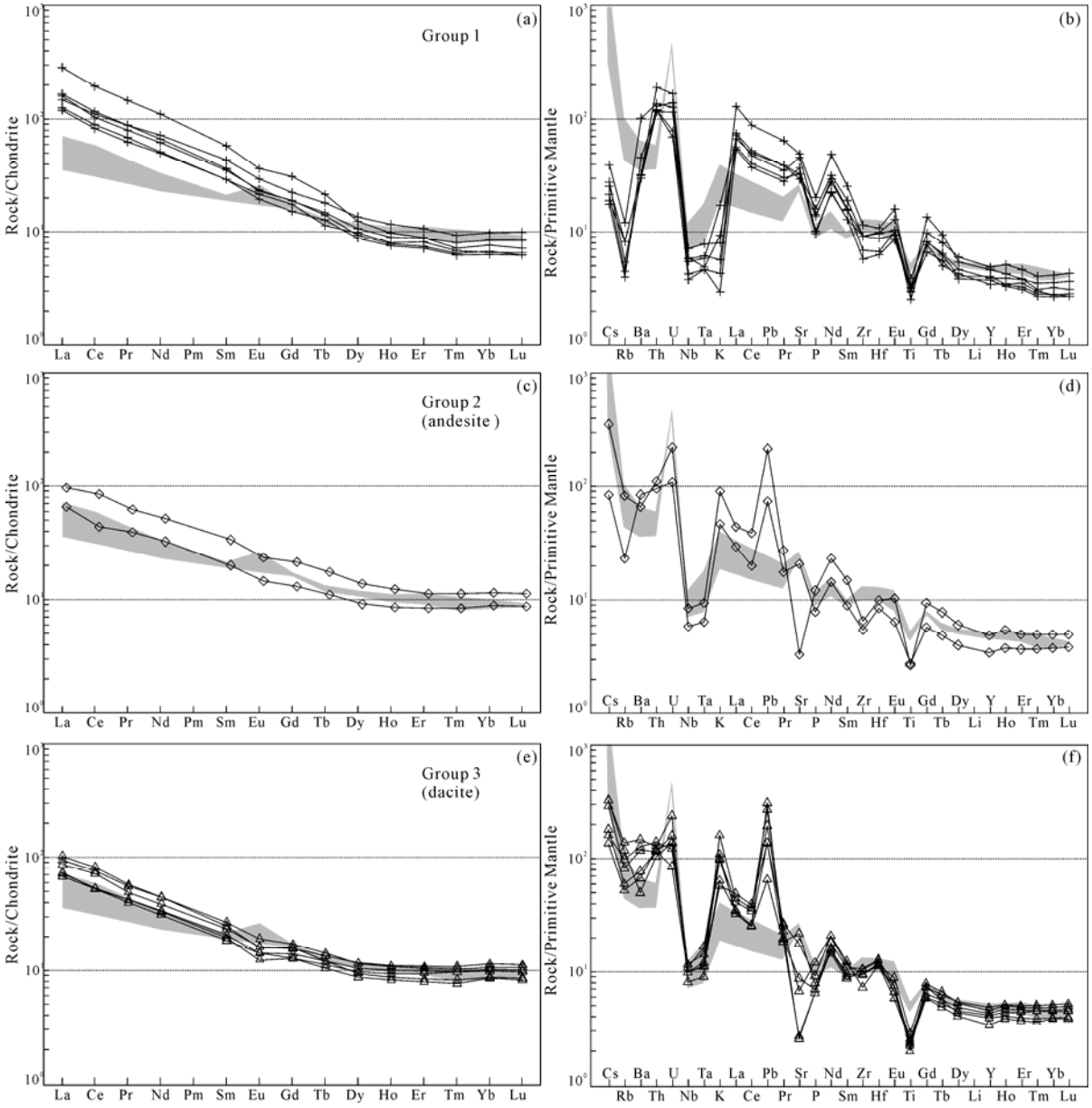

Fig. 9. Primitive mantle-normalized trace element spidergrams (Sun and McDonough, 1989) and Chondrite-normalized REE patterns (Boynton, 1984).
The shaded area data are from (Wang, 2018).

magma evolution. Although andesite and dacite are adjacently in the field, they had different magma source, different Rb/Ti ratio (0.004–0.015, 0.011–0.024 for group 2 and 3, respectively) can also proof it (Li et al., 2003). Besides, higher La/Nb ratio (mean=4.91) than lower crust (1.20, Taylor and McLennan, 1985) also suggest the addition of fluid (Condi, 1999).

As shown above, the Permian volcanic rocks in BAB are characterized by variable SiO_2 contents and a rock association of basalt, basaltic andesite, andesite, and dacite. In the La/Ba vs. La/Nb pattern (Fig. 12b), basalt to andesite samples was plotted on the lower right, deviating from OIB and evolve to the direction of subduction-modified continental lithospheric mantle (CLM), which reflect an addition of fluid. Slight Eu anomaly in chondrite normalized REE patterns (Figs. 9a, 9c, 9e) and no obvious correlation between SiO_2 and other major and trace elements suggest a low degree fractional crystallization process. Meanwhile, La/Sm vs. La pattern (Fig. 12c) illustrates that partial melting of mantle dominated the magma evolution. From above it could be seen that all basalts and andesite are mainly mantle-derived and most of them originate from depleted mantle (Fig. 12a). It is also indicated by the Lu/Hf vs. La/Sm pattern (Fig. 12d) which is usually used to estimate the depth and melting degree of basic volcanic rocks. It shows that basic rocks were the product of mantle melting at a degree lower than 5% and that all of them were in the field of spinel

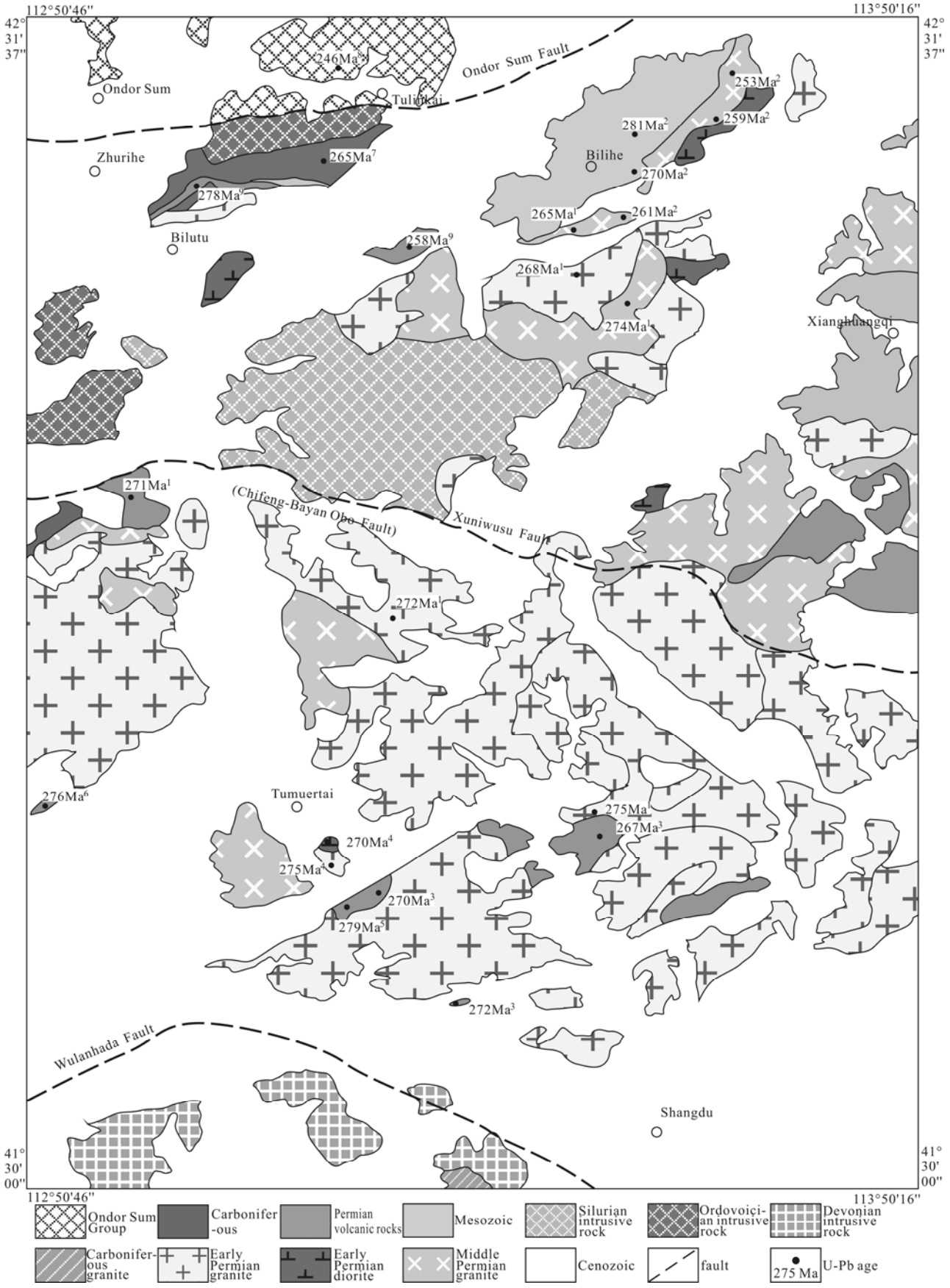

Fig. 10. Distribution map of Permian volcanic and plutonic BAB and NCB.

Modified from the geological map (scale, 1:250 000) of Sonid Right Banner and Jining region (Data sources: 1. Wang, 2014; 2. Yang et al., 2016; 3. Dong et al., 2016; 4. Wang, 2018; 5. Wang et al., 2018; 6. Zhang S H, et al., 2016; 7. Wang et al., 2017; 8. Chu et al., 2013; 9. This study).

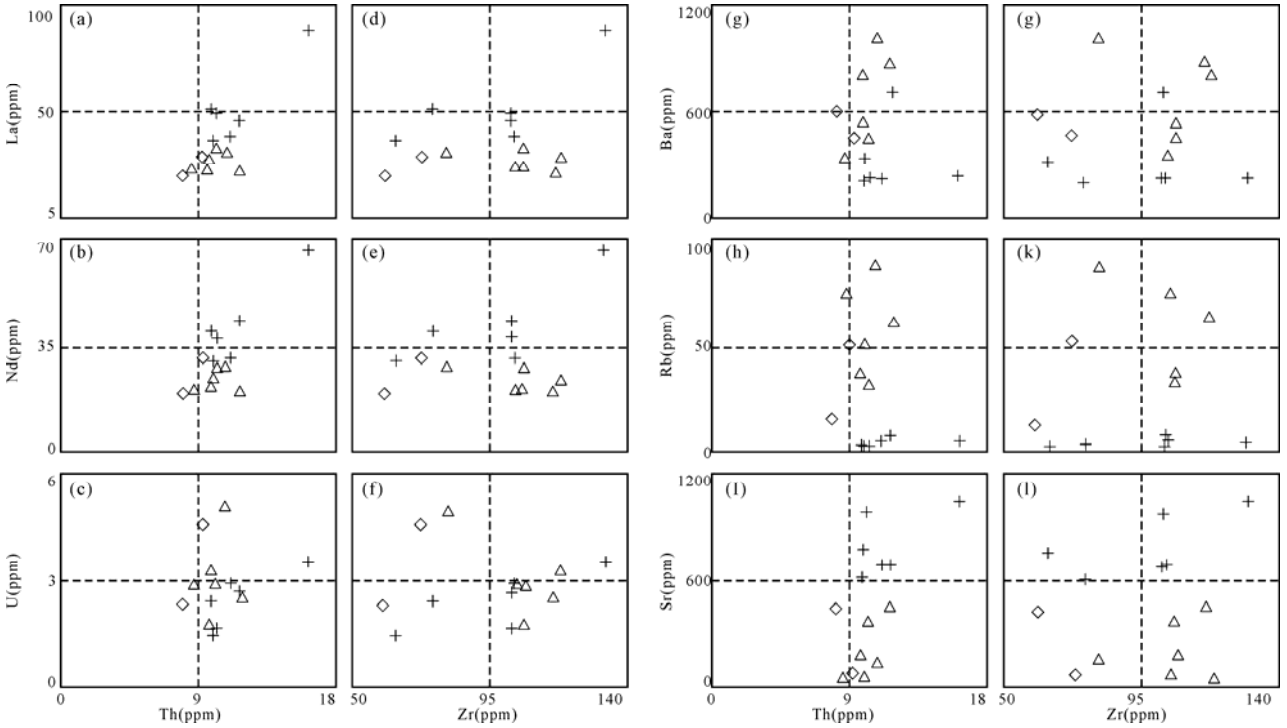

Fig. 11. Selected trace elements vs. Zr and Th diagrams for checking element mobility during post-eruptive alteration (unit ppm).

lherzolite at low pressure (Regelous et al., 2003). The $(La/Sm)_{CN}$ vs $(Tb/Yb)_{CN}$ pattern (Fig. 12e) also reveals that source area was mainly in spinel peridotite facies (Zhang et al., 2008). In summary, the basalts, and andesite in BAB formed in a low degree of mantle melting source with crustal involved in subsequent raising process. Meanwhile, the dacite was mainly from the partial melting of crust, then affected by mantle. In each magma evolution, fluid was involved, and it may be from subducted slab-derived during Permian (Cao et al., 2012).

6.3 Tectonic setting

Almost all the Permian volcanic rocks in this study belong to low-K to tholeiite or calc-alkaline to high K calc -alkaline series and show enrichment in LREE and LILE, depletion in HREE an HFSE, which reflect the characteristics of subduction zone and an arc magmatic affinity (Stern and Killian, 1996). Although some samples have high Sr and low Y values, combining this rock association and Sr/Y vs. Y pattern (Fig. 12f), it could be considered that the volcanic rocks belong to typical arc type rather than adakite. The rock-associated features of high $Mg^{\#}$ value and typical arc also display a tectonic setting of active continental margin (Deng et al., 2007). Meanwhile, the Zr/Y ratios suggest that the rocks belong to continental arc rather than ocean arc (Fig. 13a). In the Th-Hf/3-Ta diagram (Fig. 13b), they are plotted in the field of destructive plate-margin basalts field. Simultaneously, in the Y+Rb vs Rb diagram (Fig. 13c), dacites are plotted in the field of volcanic arc. All the evidence illustrates that the BAB had become an active continental margin arc during 278–258 Ma.

6.4 Temporal and spatial differences of Permian volcanic rocks

6.4.1 Differences of contemporary rocks in BAB and NCB

Basaltic andesite was chosen from Suji formation (Wang., 2018, and all related data therein) as a reference which is located only about 35 km south of Bilutu (Fig. 1, Fig. 10). The same lithology and age (279 Ma) can better constrain the differences between them. First, the component of zircons from BAB rocks is more various than NCB. There are older zircons (Figs. 6a, 6c) ages of 300–500Ma, 1000–1600 Ma, >1800 Ma in BAB. The 300 –500 Ma and >1800 Ma may represent BAB magmatism in early Paleozoic (Zhang et al., 2014; Bai et al., 2015) and the basement of NCB (Zhao et al., 2001) respectively. The 1000–1600 Ma may derive from a Gondwana fragment and they are always absent in NCB (Rojas-Agramonte et al., 2011). Meanwhile, the zircons in NCB are convergent and even the zircons ages of 1800 Ma is rare (Zhang S H, et al., 2016). Therefore, it is suggested that the BAB and NCB have different basements but have become an integrated whole before ca. 280 Ma. Second, the $\varepsilon_{Hf}(t)$ value of BAB (−6.6–6.4) is higher than NCB (−19.50 to −13.83), single-stage (T_{DM1}) of BAB (1243–757 Ma) is also younger than NCB (1497–1771 Ma) (Fig. 7), indicating different magma sources. They were influenced mainly by partial melting of the Paleoproterozoic ancient crust and lower arc continental crusts in NCB and BAB respectively. Third, rocks in BAB have lower K_2O (0.09–0.52, 0.20–1.13) and higher Sr/Y ratios (31.09–54.80, 22.24–27.97) than those in NCB. According to the polarity of subduction, K content increases from ocean to continent, from shallow to deep (Morris et al, 2003),

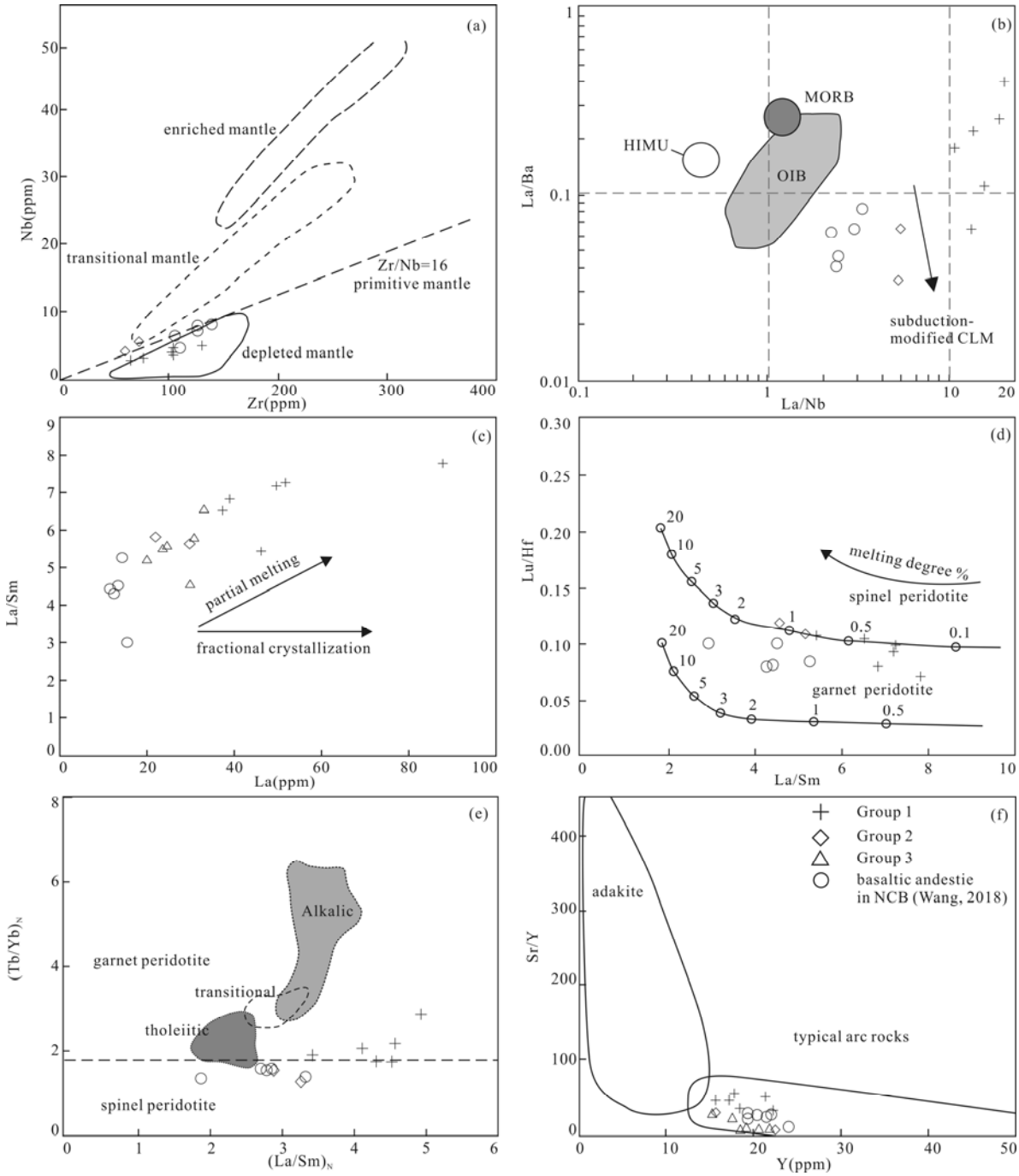

Fig. 12. (a) Nb vs. Zr; (b) La/Ba vs. La/Yb; (c) La/sm vs. La; (d) Lu/Hf vs. La/Sm; (e) $(Tb/Yb)_N$ vs. $(La/Sm)_N$; (f) Sr/Y vs. Y. (a) the reference field from (Le Roex et al., 1983); (b) the reference field from (Saunders et al., 1992); (c) the linear model from (Allègre and Minster, 1978); (d) melting degree and line represented by (Regelous et al.,2003); (e) the reference field from (Zhang et al., 2008); (f) the reference field from (Defant and Drummong, 1990).

which suggests that BAB is closer to trench; however, the subduction depth is lower than NCB, which proves there is southward subduction of PAO. The Sr/Y ratios can be used to reflect the pressure conditions of the magma source (Martin et al. 2005). High ratios of rocks in BAB represented high pressure than those in NCB though they had a lower melting degree (Figs. 12d, 12e), which may also be a reason for complex constitute of zircons. Fourth, different fractional crystallization is mainly indicated by Eu anomaly. The positive and negative δEu of NCB and BAB respectively (Fig. 9a) represent different tracks of plagioclase in magma source. So, rocks in NCB undertook a higher degree of fractional crystallization which may be related to the deeper depth of the magma.

6.4.2 Differences of asynchrony rocks (group1 and group 2) in BAB

Although there are many similarities between

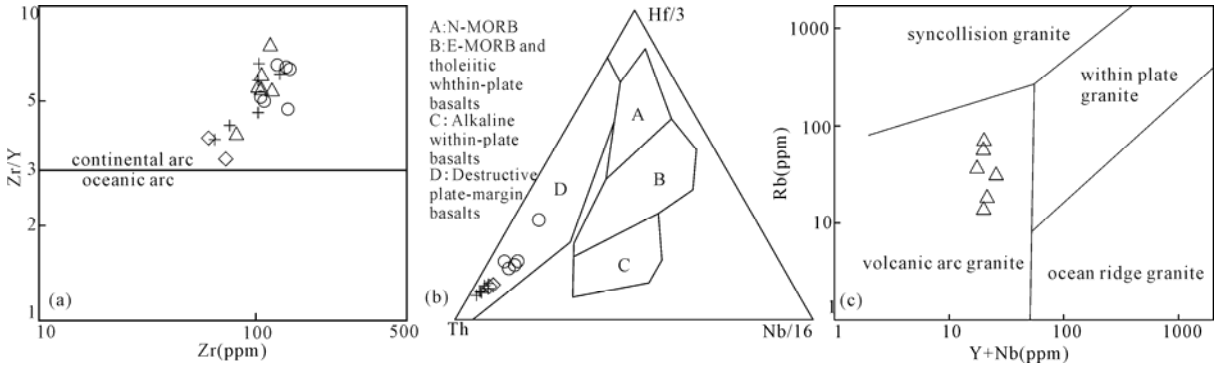

Fig. 13. The tectonic discrimination diagrams for the volcanic rocks in this study.
(a) Zr/Y vs Zr diagram after (Pearce, 1983); (b) the reference field from (Wood et al., 1979) ;(c) Rb vs Y+Rb diagram after (Pearce et al., 1984).

asynchrony rocks (group1 and group2) in BAB, some differences can still reflect the evolution of BAB during Permian. First, the ca. 270 Ma aged zircons also appeared in the younger rocks and zircons ages of ca. 250–280 Ma distribute widely in these two groups, suggesting a continuous magmatism in BAB during this period, which is also consistent with the massive magma events in NCB (Zhang S H et al., 2009, 2016). Second, the maturity of younger arc volcanic rocks (group 2) is higher than the older (group 1), which is indicated by higher K_2O values. It also suggests that the distance between the study area and the ocean trench had become farther since 278 Ma. In addition, the ages of igneous rocks zircons become younger from south to north, such as 246 Ma (Chu et al., 2013), 265 Ma (Wang et al., 2017) zircons in Ondor Sum, and 256 Ma (the youngest one in this study), which are absent in NCB on the same longitude so far. Figure 10 shows that most ages of igneous rocks in BAC are younger than those in NCB. All the facts mentioned above may imply a lateral accretion process of crust. Third, two groups of the rocks have different mantle source as shown in (Figs. 12a). The older rocks fall into the field of the depleted mantle while some younger ones are plotted on the Zr/Nb=16 line that may suggest an influence of enriched mantle at the transition of tectonic setting(Yang et al., 2016; Zhang et al., 2009a).

6.5 Geological implications

As is mentioned above, it is suggested that both the NCB and BAB belonged to an active subduction-related margin as an integrated whole in Permian though they have a different basement. There was southward subduction of the PAO beneath the BAB and NCB and the PAO closed later than 258 Ma at least. Combing massive late Carboniferous to Permian igneous rocks with characteristics of active continental margin arcs (Zhang S H, et al., 2016; Wang et al., 2018; Dong et al., 2016) which presented an extrusion setting (Table. 4). So, more evidence is required to define the existence of an ocean basin formed in middle Inner Mongolia at early Permian after the PAO closed in Devonian (Chu et al.,2014; Xu et al., 2013). Moreover, the increment of K ratios from 278–258 Ma probably indicates that an accretionary process dominated the evolution of CAOB although it is neither

Table 4 Summary ages of the Permian to early Mesozoic ingenious rocks in the NCB and BAC

Sample No	Location	Rock type	Age(Ma)	Method	Tectonic setting	References
D490	Boluono	amphibole gabbro	297	LA-ICP-MS	subduction	Zhang et al., 2009c
WZ08	Wulatezhongqi	granodiorite	291	SHRIMP	----------	Luo et al., 2007
D464	Wudaoyingzi	diorite	283	LA-ICP-MS	subduction	Zhang et al., 2009b
T1	Wulatezhongqi	monzonite granite	279	LA-ICP-MS	subduction	Wang, 2014
G3117	Tumuertai	basaltic andestie	279	LA-ICP-MS	subduction	Wang, 2018
JN2013-12	Bilutu	basaltic andestie	278	LA-ICP-MS	subduction	This study
D252	Xianghuangqi	gabbro	276	SHRIMP	subduction	Zhang et al., 2009b
07057-1	Sanjingquan	rhyolitic tuff	276	LA-ICP-MS	subduction	Zhang et al., 2016
P02B8	Honggeertu	rhyolitic tuff	275	LA-ICP-MS	subduction	Wang, 2014
P27N2-1	Tumuertai	granodiorite	275	SHRIMP	subduction	Wang et al., 2018
JN35	Gehuasitai	quartz diorite	272	LA-ICP-MS	subduction	Wang, 2014
P28N9-1	Xijingzi	rhyolite	270	LA-ICP-MS	subduction	Dong et al., 2016
P27N9-4	Tumuertai	gabbro	270	LA-ICP-MS	subduction	Wang et al., 2018
P2B8-2	Tunkendui	rhyolitic tuff	267	LA-ICP-MS	subduction	Dong et al., 2016
JN51	Bilihe	alkali-feldspar granite	265	LA-ICP-MS	transition	Wang, 2014
007-136	Bilihe	diorite porphyrite	263	LA-ICP-MS	subduction	Yang et al., 2016
B1-2	Bilihe	diorite porphyrite	259	LA-ICP-MS	subduction	Yang et al., 2016
TW0111	Bilutu	andesite	258	LA-ICP-MS	subduction	This study
BLH08-4	Bilihe	syenogranite	253	LA-ICP-MS	sys-post collision	Yang et al., 2016
X4159TW	Xiwuqi	syenogranite	259	LA-ICP-MS	post collision	Bao et al., 2007
WET14	Siziwangqi	monzonitic granite	256	LA-ICP-MS	post collision	Liu et al., 2011
11XL-4.1	Linxi	granodiorite	251	SHRIMP	sys-post collision	Li et al., 2017
11XF-6	Linxi	granodiorite	245	SHRIMP	sys-post collision	Li et al., 2017

linear nor purely accretionary process (Briggs et al., 2009; Li et al., 2016). Further, many researches have revealed that the tectonic setting has begun to transit from subduction to syn-post collision since late Permian which is supported by discovered highly fractionated I-type and high-temperature A-type granite after early Triassic in CAOB (Zhang et al., 2009; Wang, 2014; Liu et al, 2011; Listed in Table 4). Moreover, it could also be proved by extensive thrust faults which crossed late Permian plutons at the latest (Li et al., 2012; Bai, 2015). Figures 14a and 14b show an intuitive sketch map of the evolution of BAB and NCB in Permian. During early-middle Permian, dehydration of southward subduction of the PAO slab resulted in hydration and partial melting of the subcontinental lithospheric mantle wedge. These mantle-derived magmas were influenced by different crustal materials or heat the curst to form diverse volcanic rocks when erupting out of earth surface. At the end of Permian, the PAO has nearly disappeared. The BAC and NCB came into a sys-post collision and the lower crust melted to produce extensional granite as Table. 4 shows.

7 Conclusions

The geological, geochronological, geochemical, and Lu-Hf isotopic study presented thereby leads to the following conclusions:

(1) New LA-ICP-MS zircon U-Pb dating indicates that both groups of the volcanic rocks in BAB formed at 278.2±4.1 Ma and 258.3±3.0 Ma respectively, which had been mistaken as Bainaimiao group formation previously. Referring to the recent corrective age data, it could be concluded that there were obvious volcanic events in BAB during Permian.

(2) Geochemical analysis suggests that basalt to andesite were from partial melting of mantle wedge at a low degree of spinel phase and involved with crustal materials. Meanwhile, the dacites were mainly from the partial melting of crust and effected by mantle magma. And each magma evolution is in a setting of subduction with the addition of fluid.

(3) Composition of zircon and isotopic indicate that BAB and NCB have become an integrated whole before 278 Ma though they have different basements. The volcanic rocks in BAB and NCB also have different sources that reflect a lateral accretion process in a situation of southward subduction of PAO.

(4) These volcanic rocks have provided convincing evidence that NCB and BAB belong to active continental margin and the PAO has not closed yet until 258 Ma. The PAO disappeared gradually and the CAOB got into a condition of syn-post collision during the late Permian to Triassic.

Acknowledgments

We gratefully acknowledge the editor Prof. Li Shan for his work about this study. We thank the anonymous reviewers for a thorough revision of the manuscript. This work was supported by the National Natural Science Foundation of China (41872203, 41872194), and the China Geological Survey Project (DD2016041–16,

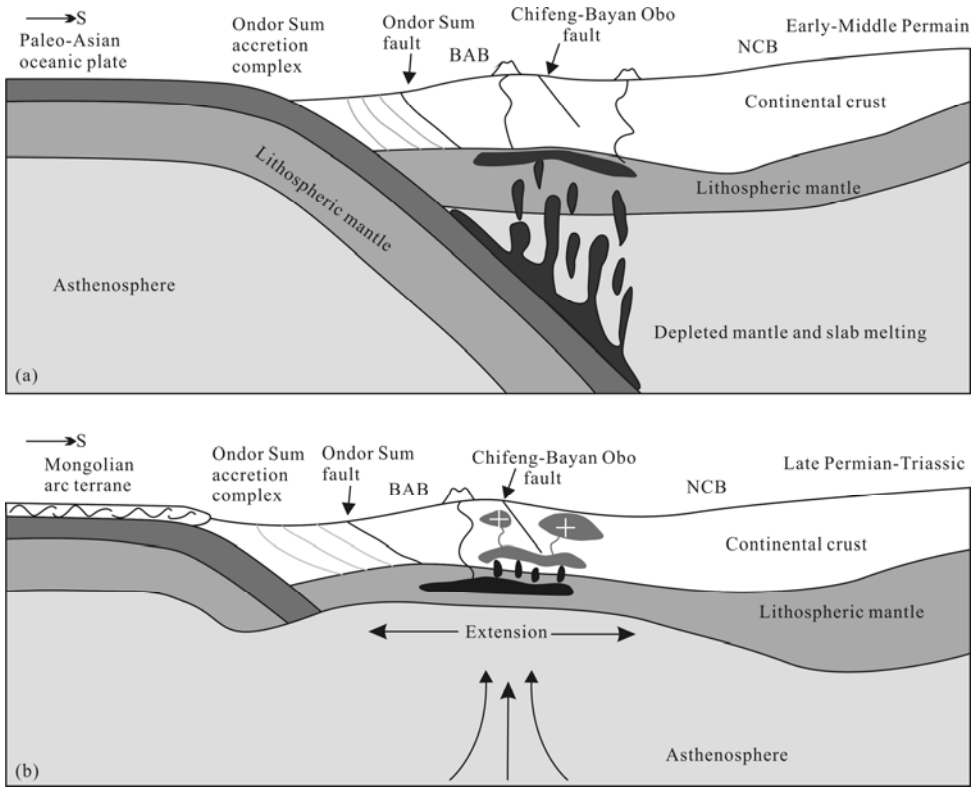

Fig. 14. Schematic cartoons showing the tectonic setting and petrogenetic model of the volcanic rocks in Bainaimiao arc belt in Permian (modified from Zhang et al., 2009a).

DD20190038–2)

Manuscript received May 15, 2019
accepted Aug. 14, 2019
associate EIC XIAO Wenjiao
edited by LIU Lian

References

Allègre, C.J., and Minster, J.F., 1978. Quantitative models of trace element behavior in magmatic processes. Earth and Planetary Science Letters, 38(1): 1–25.

Andersen, T., 2002. Correction of common lead in U–Pb analyses that do not report ^{204}Pb. Chemical Geology, 192(1): 59–79.

Bai, X.H., 2015. Tectonic deformation of the Xuniwusu thrusting tectonic systems in Inner Mongolia (Master. thesis). Changchun: Jilin University, 1–73 (in Chinese with English abstract).

Bai, X.H., Xu, Z.Y., Liu, Z.H., Xin, H.T., Wang, W.Q., Wang, X., and Lei, C.C., 2015. Zircon U-Pb dating, geochemistry and geological significance of the early Silurian plutons from the southeastern margin of the Central Asian Orogenic Belt. Acta Petrologica Sinica, 31(1): 67–79 (in Chinese with English abstract).

Bao, Z.Q., Zhang, C.J., Wu, Z.L., Wang, H., Li, W., Sang, J.H., Liu, Y.S., 2007. Zircon SHRIMP U-Pb dating of granitoids in Late Paleozoic rift area, southeastern Inner Mongolia, and its implications. Geology in China, 34(5): 790–798 (in Chinese with English abstract).

Belousova, E.A., Griffin, W.L., O'Reilly, S.Y., and Fisher, N.I., 2002. Igneous zircon: trace element composition as an indicator of source rock type. Contributions to Mineralogy & Petrology, 143(5): 602–622.

Boyton, W.V., 1984. Cosmochemistry of the rare earth studies: meteorite studies. Developments in Geochemistry, 63–114.

Briggs, S., Yin, A., Manning, C.E., Chen, Z.L., and Wang, X.F., 2009. Tectonic development of the southern Chinese Altai Range as determined by structural geology, thermobarometry, ^{40}Ar/^{39}Ar thermochronology, and Th/Pb ion-microprobe monazite geochronology. Geological Society of America Bulletin, 121(9–10): 1381–1393.

Bureau of Geology and Mineral Resources of Inner Mongolia (BGMRIM), 1991. Regional geology of Nei Mongol (Inner Mongolia) autonomous region. Beijing: Geological Publishing House, 1–725 (in Chinese with English abstract).

Cao, H.H., Xu, W.L., Pei, F.P., Guo, P.Y., Wang, F., 2012. Permian tectonic evolution of the eastern section of the northern margin of the North China Plate: Constraints from zircon U-Pb geochronology and geochemistry of the volcanic rocks. Acta Petrologica Sinica, 28(9): 2733–2750 (in Chinese with English abstract).

Chen, C., Ren, Y.S., Zhao, H.L., Zou, X.T., Yang, Q., and Hu, Z.C., 2014. Permian age of the Wudaogou Group in eastern Yanbian: detrital zircon U-Pb constraints on the closure of the Paleo–Asian Ocean in Northeast China. International Geology Review, 56(14): 1754–1768.

Chen, M., Sun, M., Buslov, M.M., Cai, K.D., Zhao, G.C., Kulikova, A.V., and Rubanova, E.S., 2016. Crustal melting and magma mixing in a continental arc setting: Evidence from the Yaloman intrusive complex in the Gorny Altai terrane, Central Asian Orogenic Belt. Lithos, 252–253: 76–91.

Chu, H., Zhang, J.R., Wei, C.J., Wang, H.C., and Ren, Y.W., 2013. A new interpretation of the tectonic setting and age of meta-basic volcanics in the Ondor Sum Group, Inner Mongolia. Chinese Science Bulletin, 58(28–29): 3580–3587.

Condie, K.C., 1999. Mafic crustal xenoliths and the origin of the lower crust. Lithos, 46(1): 95–101.

Defant, M. J. and Drummond, M.S., 1990. Derivation of some modern arc magmas by melting of young subducted lithosphere. Nature, 347(6294): 662–665.

Deng, J.F., Xiao, Q.H., Su, S.G., Liu, C., Zhao, G.C., Wu, Z.X., and Liu, Y., 2007. Igneous petrotectonic assemblages and tectonic settings: A discussion. Geological Journal of China Universities, 13(3): 392–402 (in Chinese with English abstract).

Dong, X.J., Wang, W.Q., Sha, Q., and Zhang, J.F., 2016. Suzy volcanic rocks in the northern margin of the North China Craton and its formation mechanism. Acta Petrologica Sinica, 32(9): 2765–2779 (in Chinese with English abstract).

Eizenhöfer, P.R. and Zhao, G.C., 2018. Solonker Suture in East Asia and its bearing on the final closure of the eastern segment of the Palaeo-Asian Ocean. Earth-Science Reviews, 186: 153–172.

Eizenhöfer, P.R., Zhao, G.C., Zhang, J., and Sun, M., 2014. Final closure of the paleo–Asian Ocean along the Solonker suture zone: constraints from geochronological and geochemical data of Permian volcanic and sedimentary rocks. Tectonics, 33: 441–463.

Gibson, I.L., Kirkpatrick, R.J., Emmerman, R., Schmincke, H.U., Pritchard, G., Oakley, P.J., Thorpe, R.S., and Marriner, G.F., 1982. The trace element composition of the lavas and dikes from a 3 km vertical section through the lava pile of eastern Iceland. Journal of Geophysical Research Solid Earth, 87(B8): 6532–6546.

Griffin, W.L., Wang, X., Jackson, S.E., Pearson, N.J., O'Reilly, S.Y., Xu, X., and Zhou, X.M., 2002. Zircon chemistry and magma mixing, SE China: In-situ analysis of Hf isotopes, Tonglu and Pingtan igneous complexes. Lithos, 61(3–4): 237–269.

Guan, Q.B., Liu, Z.H., Liu, Y.J., Liu, J., Wang, S.J., and Tian, Y., 2018. Geochemistry and zircon U-Pb geochronology of mafic rocks in the Kaiyuan tectonic mélange of northern Liaoning Province, NE China: Constraints on the tectonic evolution of the Paleo-Asian Ocean. Geological Journal, 2019 (54): 656–678.

Hou, K.J., Li, Y.H., Zou, T.R., Qu, X.M., Shi, Y.R., and Xie, G.Q., 2007. Laser ablation-MC-ICP-MS technique for Hf isotope microanalysis of zircon and its geological applications. Acta Petrologica Sinica, 23(10): 2595–2604 (in Chinese with English abstract).

Hou, K.J., Li, Y.H., and Tian, Y.R., 2009. In situ U-Pb zircon dating using laser ablation-multi counting-ICP-MS. Mineral Deposits, 28(4): 184–192 (in Chinese with English abstract).

Hu, X., Xu, C.S., and Niu, S.Y., 1990. Evolution of the early Paleozoic continental margin in northern margin of the North China Platform. Beijing: Beijing University Press, 1–215 (in Chinese with English abstract).

Jahn, B.M., Wu, F.Y., and Chen, B., 2000. Granitoids of the Central Asian Orogenic Belt and continental growth in the Phanerozoic. Transactions of the Royal Society of Edinburgh: Earth Sciences, 91(1–2): 181–193.

Jian, P., Liu, D.Y., Kröner, A., Windley, B.F., Shi, Y.R., Zhang, F.Q., Shi, G.H., Miao, L.C., Zhang, W., Zhang, Q., Zhang, L.Q., and Ren, J.S., 2008. Time scale of an early to mid-Paleozoic orogenic cycle of the long-lived Central Asian Orogenic Belt, Inner Mongolia of China: Implications for continental growth. Lithos, 101(3): 233–259.

Jian, P., Liu, D.Y., Kröner, A., Windley B.F., Shi, Y.R., Zhang W., Zhang, F.Q., Miao, L.C., Zhang, L.Q., and Tomurhuu, D., 2010. Evolution of a Permian intraoceanic arc-trench system in the Solonker suture zone, Central Asian Orogenic Belt, China and Mongolia. Lithos, 118(1–2): 169–190.

Jong, K.D., Xiao, W.J., Windley, B.F., Masago, H., and Lo, C.H., 2006. Ordovician ^{40}Ar/^{39}Ar phengite ages from the blueschist-facies Ondor Sum subduction-accretion complex (Inner Mongolia) and implications for the early Paleozoic history of continental blocks in China and adjacent areas. Journal of Science, 306(12): 799–845.

Koschek, S., 1993. Origin and significance of the SEM cathodoluminescence from zircon. Journal of Microscopy, 171 (3): 223–232.

Le Bas, M.J., Le Maitre, R.W., Streckeisen, A., and Zanettin, B., 1986. A chemical classification of volcanic rocks based on the total alkali-silica diagram. Journal of Petrology, 27(3): 745–750.

Le Roex, A.P., Dick, H.J.B., Erlank, A.J., Reid, A.M., Frey, F.A., and Hart, S.R., 1983. Geochemistry, mineralogy and petrogenesis of lavas erupted along the southwest Indian

Ridge between the Bouvet Triple Junction and 11 Degrees East. Journal of Petrology, 24(3): 267–318.
Li, S., Wang, T., Wilde, S.A., Tong, Y., 2013. Evolution, source and tectonic significance of Early Mesozoic granitoid magmatism in the Central Asian Orogenic Belt (central segment). Earth-Science Reviews, 126: 206–234.
Li, S., Wilde, S.A., He, Z., Jiang, X., Liu, R., Zhao, L., 2014. Triassic sedimentation and post accretionary crustal evolution along the Solonker suture zone in Inner Mongolia, China. Tectonics, 33(6): 960–981.
Li, S., Chung, S.L., Wilde, S.A., Wang, T., Xiao, W.J., Guo, Q.Q., 2016. Linking magmatism with collision in an accretionary orogen. Scientific Reports, 6(1): 25751.
Li, S., Chung, S.L., Wilde, S.A., Jahn, B.M., Xiao, W.J., Wang, T., Guo, Q.Q., 2017. Early-Middle Triassic high Sr/Y granitoids in the southern Central Asian Orogenic Belt: Implications for ocean closure in accretionary orogens. Journal of Geophysical Research: Solid Earth, 122: 2291–2309.
Li, C.D., Ran, G., Zhao, L.G., Wang, H.C., Zhang, K., Xu, Y.W., Gu, Y.C., and Zhang, Y.Q., 2012. LA-MC-ICP MS U-Pb geochronology of zircons from the Wenduermiao Group and its tectonic significance. Acta Petrologica Sinica, 28(1): 3702–3714 (in Chinese with English abstract).
Li, G., Liu, Z.H., Xu, Z.Y., Peng, X.D., Dong, X.J., Sha, Q., and Wang, W.Q., 2012. Components of the Bainaimiao thrust and its structural features. Journal of Jilin University (Earth Science Edition), 42(2): 309–319 (in Chinese with English abstract).
Li, J.Y., 2006. Permian geodynamic setting of Northeast China and adjacent regions: closure of the Paleo-Asian Ocean and subduction of the Paleo-Pacific Plate. Journal of Asian Earth Sciences, 26(3–4): 0–224.
Li, Y.J., Zhao, R.F., Li, Z.C., Liu, Z.W., Li, Y., 2003. Origin discrimination of granitoids formed by mingled magma: Using a trace element diagram and exemplified by Wenquan granites，western Qinling. Journal of Chang'an University (Earth Science Edition), 25(3): 7–12 (in Chinese with English abstract).
Lin, W., Faure, M., Nomade, S., Shang, Q.H., and Renne, P.R., 2008. Permian-Triassic amalgamation of Asia: Insights from Northeast China sutures and their place in the final collision of North China and Siberia. Comptes Rendus–Geoscience, 340(2–3): 190–201.
Liu, C. F., Zhou, Z. G., Zhang, H. F., Liu, W.C., Zhang, L., 2011. Petrochemical characteristics and timing of Wuertagaolemiao granitoids, Siziwangqi, Inner Mongolia. Journal of Mineralogy and Petrology, 31(4): 34–43 (in Chinese with English abstract).
Liu, C.F., Liu, W.C., and Zhou, Z.G., 2014. Geochronology, geochemistry and tectonic setting of the Paleozoic-Early Mesozoic intrusive in Siziwangqi, Inner Mongolia. Acta Geologica Sinica, 88(6): 992–1002 (in Chinese with English abstract).
Liu, D.Y., Jian, P., Zhang, Q., Zhang, F.Q., Shi, Y.R., Shi, G.H., Zhang, L.Q., Tao, H., 2003. SHRIMP dating of adakites in the Tulingkai ophiolite, Inner Mongolia: evidence for the early Paleozoic subduction. Acta Geologica Sinica, 77(3): 317–327 (in Chinese with English abstract).
Luo, H.L., Wu, T.R., Li, Y., 2007. Geochemistry and SHRIMP Dating of the Kebu Massif from Wulatezhongqi, Inner Mongolia: Evidence for the Early Permian Underplating beneath the North Chian Craton. Acta Petrologica Sinca, 23 (4): 755–766 (in Chinese with English abstract).
Ludwig, K.R., 2003. User's manual for Isoplot 3.00: a geochronological toolkit for Microsoft Excel. Berkeley Geochronology Center Special Publication, 4: 1–70.
Martin, H., Smithies, R.H., Rapp, R., Moyen, J.F., and Champion, D., 2005. An overview of adakite, tonalite-trondhjemite-granodiorite (TTG), and sanukitoid: relationships and some implications for crustal evolution. Lithos, 79(1–2): 1–24.
Morris, J.D., and Ryan, J.G., 2003. Subduction zone processes and implications for changing composition of the upper and lower mantle. Treatise on Geochemistry, Pergamon Oxford: 451–470.
Peacock, S.M., Rushmer, T., and Thompson, A.B., 1994. Partial melting of subducting oceanic crust. Earth & Planetary Science Letters, 121(1–2): 227–244.
Pearce, J.A., 1983. Role of the sun-continental lithosphere in magma genesis at active continental margins. In: Hawkesworth C J Norry M J (eds). Continental Basalts and Mantle Xenoliths. Nantwich: Shiva: 230–249.
Pearce, J.A., Harris, N.B.W., Tindle, A.G., 1984. Trace element discrimination diagrams for the tectonic interpretation of granitic rocks. Journal of Petrology, 25(4): 956–983.
Peccerillo, A., and Taylor, S.R., 1976. Geochemistry of Eocene calc-alkaline volcanic rocks from the Kastamonu area, northern Turkey. Contributions to Mineralogy and Petrology, 58(1): 63–81.
Qing, M., Tang, M.G., Ge, L.S., Han, X.J., Feng, J.B., Yuan, S.S., and Zhao, Y.S., 2012. LA-ICP-MS zircon U-Pb age, geochemistry of andesite in Bilihe goldfield, Suniteyouqi, Inner Mongolia and its tectonic significance. Acta Petrologica Sinica, 28(2): 514–524 (in Chinese with English abstract).
Regelous, M., Hofmann, A.W., Abouchami, W., Galerie, and S.J.G.,2003. Geochemistry of lavas from the Emperor seamounts, and the geochemical evolution of Hawaiian magmatism from 85 to 42 Ma. Journal of Petrology, 44(1): 113–140.
Rojas-Agramonte, Y., Kroner, A., Demoux, A., Xia, X., Wang, W., Donskaya, T., Liu, D., and Sun, M., 2011. Detrital and xenocrystic zircon ages from Neoproterozoic to Paleozoic arc terranes of Mongolia: Significance for the origin of crustal fragments in the Central Asian Orogenic Belt. Gondwana Research, 19(3): 751–763.
Rosler, H.J., and Beuge, P., 1983. Geochemistry of trace elements during regional metamorphism. In: Augustithis S (ed), The significance of trace elements in solving petrogenetic problems and controversies. Athen: Theophrastus: 407–430.
Saunders, A.D., Storey, M., Kent, R.W., and Norry, M.J., 1992. Consequences of plume-lithosphere interactions. Geological Society, 68(1): 41–60.
Sengör, A.M.C., Natal'In, B.A., and Burtman, V.S., 1993. Evolution of the altaid tectonic collage and Paleozoic crustal growth in Eurasia. Nature, 364(6435): 299–307.
Stern, C.R., and Kilian, R., 1996. Role of the subducted slab, mantle wedge and continental crust in the generation of adakites from the Andean Austral Volcanic Zone. Contributions to Mineralogy & Petrology, 123(3): 263–281.
Sun, S.S., and McDonough, W.F., 1989. Chemical and isotopic systematics of oceanic basalts: Implications for mantle composition and processes. Geological Society London Special Publications, 42(1): 303–345.
Tang, K.D., 1990. Tectonic development of Paleozoic fold belts at the north margin of the Sino-Korean Craton. Tectonics, 9 (2): 249–260.
Tang, K.D., and Yan, Z.Y., 1993. Regional metamorphism and tectonic evolution of the Inner Mongolian suture zone. Journal of Metamorphic Geology, 11(4): 12.
Taylor, S.R., and McLennan, S.M., 1985. The continental crust: Its composition and evolution. Oxford, UK: Blackwell Science Publication: 1–321
Wang, G.S., Wu, C., Chen, C., Zhou, Z.G., Liu, C.F., and Jiang, T., 2017. Geochronological data of igneous and metamorphic rocks from the Xing'an-Mongolia Orogenic Belt of the eastern Central Asian Orogenic Belt: Implications for the final closure of the Paleo-Asian Ocean. International Journal of Earth Sciences, 106(8): 2727–2746.
Wang, Q., and Liu, X.Y., 1986. Paleo plate tectonics between Cathaysia and Angaraland in Inner Mongolia of China. Tectonics, 5(7): 1073–1088.
Wang, S.J., 2018. Permian tectono-magmatic activities and its geological significance in Tumuertai area, Inner Mongolia (Master. thesis). Changchun: Jilin University, 1–68 (in Chinese with English abstract).
Wang, S.J., Xu, Z.Y., Dong, X.J., Wang, W.Q., and Li, P.C., 2018. Geochemical characteristics and zircon U-Pb age of the granodiorite-norite gabbro in the northern margin of the North

China Block and their formation mechanism. Earth Science, 43(9): 3267–3284 (in Chinese with English abstract).
Wang, W.Q., 2014. Late Paleozoic tectonic evolution of the central-northern margin of the North China Plate: Constraints from zircon U-Pb ages and geochemistry of igneous rocks in Ondor Sum-Jining area (Ph.D. thesis). Changchun: Jilin University, 1–169 (in Chinese with English abstract).
Wilde, S.A., 2015. Final amalgamation of the Central Asian Orogenic Belt in NE China: Paleo-Asian Ocean closure versus Paleo-Pacific plate subduction-A review of the evidence. Tectonophysics, 662: 345–362.
Windley, B.F., Alexeiev, D., Xiao, W.J., Kröner. A., and Badarch, G., 2007. Tectonic models for accretion of the Central Asian Orogenic Belt Journal of the Geological Society, 164(12): 31–47.
Wood, D.A., 1979. A reappraisal of the use of trace elements to classify and discriminate between magma series erupted in different tectonic settings. Earth Planet.Sci.Lett, 45(2): 326–336.
Wu, F.Y., Yang, Y.H., Xie, L.W., Yang, J.H., and Xu, P., 2006. Hf isotopic compositions of the standard zircons and baddeleyites used in U-Pb geochronology. Chemical Geology, 234(1–2): 105–126.
Wu, F.Y., Zhao, G.C., Sun, D.Y., Wilde, S.A., and Yang, J.H., 2007. The Hulan Group: Its role in the evolution of the Central Asian Orogenic Belt of NE China. Journal of Asian Earth Sciences, 30(3–4): 542–556.
Xiao, W.J., Windley, B.F., Hao, J., and Zhai, M.G., 2003. Accretion leading to collision and the Permian Solonker suture, Inner Mongolia, China: Termination of the central Asian orogenic belt. Tectonics, 22(6): 8–1–8–21.
Xiao, W.J., Huang, B.C., Han, C.M., Sun, S., and Li, J.L., 2010. A review of the western part of the Altaids: A key to understanding the architecture of accretionary orogens. Gondwana Research, 18: 253–273.
Xiao, W.J., Windley, B., Sun, S., Li, J.L., Huang, B.C., Han, C., Yuan, C., Sun, M., and Chen, H.L., 2015. A Tale of Amalgamation of Three Permo-Triassic Collage Systems in Central Asia: Oroclines, Sutures, and Terminal Accretion. Annual Review of Earth and Planetary Sciences, 43(1): 16.1–16.31.
Xu, B., Charvet, J., Chen, Y., Zhao, P., and Shi, G.Z., 2013. Middle Paleozoic convergent orogenic belts in western Inner Mongolia (China): framework, kinematics, geochronology and implications for tectonic evolution of the Central Asian Orogenic Belt. Gondwana Research, 23(4): 1342–1364.
Yang, Z., Chang, Z., Hou, Z., and Meffre, S., 2016. Age, igneous petrogenesis, and tectonic setting of the Bilihe gold deposit, China, and implications for regional metallogeny. Gondwana Research, 34: 296–314.
Zhang, H.S., Li, Q.S., Ye, Z., Gong, C., and Wang, X.R., 2018. New seismic evidence for continental collision during the assembly of the central Asian orogenic belt. Journal of Geophysical Research: Solid Earth, 123: 6687–6702.
Zhang, J.R., Wei, C.J., and Chu, H., 2018. New model for the tectonic evolution of Xing'an-Inner Mongolia Orogenic Belt: Evidence from different phases of metamorphism in Central Inner Mongolia. Acta Petrologica Sinica, 34(10): 2857–2872 (in Chinese with English abstract).
Zhang, J.F., and Bai, X.H., 2016. The early Carboniferous volcanic rocks in Ondor Sum area of Sonid Right Banner, Inner Mongolia: Discovery and its tectonic significance. Acta Petrologica Sinica, 32(9): 2780–2792 (in Chinese with English abstract).
Zhang, S.H., Zhao, Y., Song, B., Hu, J.M., Liu, S.W., Yang, H.Y., Chen, F.K., Liu, X.M., Liu, J., 2009a. Contrasting Late Carboniferous and Late Permian-Middle Triassic intrusive suites from the northern margin of the North China craton: Geochronology, petrogenesis, and tectonic implications. Geological Society of America Bulletin, 121(121): 181–200.
Zhang, S.H., Zhao, Y., Kröner, A., Liu, X.M., Xie, L.W., Chen, F.K., 2009b. Early Permian plutons from the northern North China Block: Constraints on continental arc evolution and convergent margin magmatism related to the Central Asian Orogenic Belt. International Journal of Earth Sciences, 98(6): 1441–1467.
Zhang, S.H., Zhao, Y.，Liu, X.C, Liu, D.Y., Chen, F.K., Xie, L.W., Chen, H.H., 2009c. Late Paleozoic to early Mesozoic mafic-ultramafic complexes from the northern North China Block: Constraints on the composition and evolution of the lithospheric mantle. Lithos, 110(1): 229–246.
Zhang, S.H., Zhao, Y., Ye, H., Liu, J.M., and Hu, Z.C., 2014. Origin and evolution of the Bainaimiao arc belt: Implications for crustal growth in the southern Central Asian orogenic belt. Geological Society of America Bulletin, 126(9–10): 1275–1300.
Zhang, S.H., Zhao, Y., Liu, J.M., and Hu, Z.C., 2016. Different sources involved in generation of continental arc volcanism: The Carboniferous-Permian volcanic rocks in the northern margin of the North China block. Lithos, 240–243: 382–401.
Zhang, X.H., Zhang, H., Tang, Y., Wilde, S.A., and Hu, Z., 2008. Geochemistry of Permian bimodal volcanic rocks from central Inner Mongolia, North China: Implication for tectonic setting and Phanerozoic continental growth in Central Asian Orogenic Belt. Chemical Geology, 249(3–4): 262–281.
Zhao, G.C., Wilde, S.A., Cawood, P.A., and Sun, M., 2001. Archean blocks and their boundaries in the North China Craton: lithological, geochemical, structural and P-T path constraints and tectonic evolution. Precambrian Research, 107: 45–73.
Zhao, P., Chen, Y., Xu, B., Faure, M., Shi, G.Z., and Chooulet, F., 2013. Did the Paleo-Asian Ocean between North China Block and Mongolia Block exist during the late Paleozoic? First paleomagnetic evidence from central-eastern Inner Mongolia China. Journal of Geophysical Research: Solid Earth, 118(5): 1873–1894.
Zhou, H., Zhao, G.C., Han, Y.G., and Wang, B., 2018. Geochemistry and zircon U-Pb-Hf isotopes of Paleozoic rocks in the Damao area in Inner Mongolia, northern China: implications for the tectonic evolution of Bainaimiao arc. Lithos, 314–315: 119–139.

About the first author

WANG Shijie, male; born in 1993 in Heilongjiang, doctor; mainly engaged in tectonic geology, in Jilin University. E-mail: wangshijie1993@qq.com

About the corresponding author

DONG Xiaojie, male, born in 1984 in Hebei, lecturer; mainly engaged in tectonic geology and Precambrian geology, in Jilin University. E-mail: dxj@jlu.edu.cn